The Solar Neighborhood. XXXIII. Parallax Results from the CTIOPI 0.9m Program: Trigonometric Parallaxes of Nearby Low-Mass Active and Young Systems

Adric R. Riedel[1,2a], Charlie T. Finch[3a], Todd J. Henry[4a], John P. Subasavage[5a], Wei-Chun Jao[4a], Lison Malo[6], David R. Rodriguez[7] Russel J. White[4], Douglas R. Gies[4], Sergio B. Dieterich[4a], Jennifer G. Winters[4a], Cassy L. Davison[4a], Edmund P. Nelan[8], Sarah C. Blunt[9,2], Kelle L. Cruz[1,2],Emily L. Rice[9,2],Philip A. Ianna[10a]

[1]*Department of Physics and Astronomy, Hunter College, The City University of New York, 695 Park Avenue, New York, NY 10065*

[2]*Department of Astrophysics, American Museum of Natural History, Central Park West at 79th Street, New York, NY 10024*

[3]*Astrometry Department, U.S. Naval Observatory, Washington DC 20392*

[4]*United States Naval Observatory, Flagstaff, AZ 86001, USA*

[5]*Department of Physics and Astronomy, Georgia State University, P.O. Box 5060, Atlanta, GA 30302-5060*

[6]*Département de Physique et Observatoire du Mont-Megantic, Université de Montréal, C.P. 6128, Succursale Centre-Ville, Montréal, QC, Canada H3C 3J7*

[7]*Departamento de Astronomia, Universidad de Chile, Casilla 36-D, Las Condes, Santiago, Chile*

[8]*Space Telescope Science Institute*

[9]*Department of Engineering Science and Physics, College of Staten Island, 2800 Victory Boulevard, New York, NY 10314*

[10]*Department of Astronomy, University of Virginia, Charlottesville, VA 22904*

ar494@hunter.cuny.edu

ABSTRACT

We present basic observational data and association membership analysis for 45 young and active low-mass stellar systems from the ongoing RECONS photometry and astrometry program at the Cerro Tololo Inter-American Observatory. Most of these systems have saturated X-ray emission ($\log \frac{L_X}{L_{bol}} > -3.5$) based on X-ray fluxes from the ROSAT All-Sky Survey, and many are significantly more luminous than main-sequence stars of comparable color. We present parallaxes and proper motions, Johnson-Kron-Cousins VRI photometry, and multiplicity observations from the CTIOPI program on the CTIO 0.9m telescope. To this we add low-resolution optical spectroscopy and line measurements from the CTIO 1.5m telescope, and interferometric binary measurements from the Hubble Space Telescope Fine Guidance Sensors. We also incorporate data from published sources: JHK_S photometry from the 2MASS point source catalog; X-ray data from the ROSAT All-Sky Survey; and radial velocities from literature sources. Within the sample of 45 systems, we identify 21 candidate low-mass pre-main-sequence members of nearby associations, including members of β Pictoris, TW Hydrae, Argus, AB Doradus, two ambiguous $\approx$30 Myr old systems, and one object that may be a member of the Ursa Major moving group. Of the 21 candidate young systems, 14 are newly identified as a result of this work, and six of those are within 25 parsecs of the Sun.

1. Introduction

Over the past 20 years, a variety of loose associations have been discovered, with distances (<100 pc) much closer than any star-forming region, and ages (∼100 Myr) much younger than any comparably close moving group (e.g. Ursa Major, King et al. 2003). These associations include such well-studied groups as TW Hydra (de la Reza et al. 1989; Gregorio-Hetem et al. 1992), β Pictoris (Barrado y Navascués et al. 1999), Tucana-Horologium (Zuckerman et al. 2001), Argus (Torres et al. 2003), AB Doradus (Zuckerman et al. 2004), Carina (Torres et al. 2008), and Columba (Torres et al. 2008).

Most of the currently known members of these associations are solar-type or hotter stars, reflecting a bias toward bright stars that are surveyed in the proper motion catalogs, *HIPPARCOS* and *TYCHO-2*. We are likely left without information on most of the members of these associations; for instance, M dwarfs make up *at least* 75% of all nearby stars (Henry et al. 2006), but make up less than half of the known members of young associations (see Table 6).

The dearth of M dwarfs is a distinct issue with star formation theory, and presents difficulties with our understanding of young associations. M dwarfs, because of their lower masses, should be more easily scattered by dynamical interactions than solar-type stars, and thus the current spatial and kinematic boundaries of the associations will not necessarily contain many of the associated stars. By virtue of numbers, they will better inform the Initial Mass Function (IMF) measurements of young associations, which currently appear to be very different from the field IMF (Schlieder 2011). M dwarfs provide an advantage for exoplanet research because they are redder and dimmer, which enhances the contrast between the stars and any forming planets in their star systems. Finally, M dwarfs take significantly longer to reach the main sequence (at least 200 Myr, Dotter et al. 2008), which makes it easier to identify and obtain precise ages for young M dwarfs.

To address the issue of missing M dwarfs, we present the results of a new survey of young and active M dwarfs, as part of the Research Consortium On Nearby Stars[1] (RECONS) exploration of the Solar Neighborhood. We present 45 nearby star systems with M dwarf primaries (35 with new astrometry and photometry) observed during the Cerro Tololo Inter-American Obseratory Parallax Investigation (CTIOPI). Our analysis of youth is based on absolute trigonometric parallaxes, Johnson-Kron-Cousins VRI photometry, spectral types, variability, kinematic analyses, and surface gravity estimates. The systems discussed herein include both known and new candidate pre-main-sequence members of the β Pictoris, TW Hydra, Tucana-Horologium, Columba, Argus, AB Doradus, and Castor associations.

Identifying young stars (specifically, pre-main-sequence young stars) is a complicated process. There are many signatures of youth that can be detected in M dwarf stars. Unfortunately, there is no single indicator that completely describes youth, and none of the parameters are foolproof. Lithium equivalent widths (EWs), spectral accretion signatures, and protoplanetary disks are all only found in young stars, but they are short-lived effects, and stars can lack those properties and still be pre-main-sequence objects. Conversely, the other parameters (overluminosity, low surface gravity, chromospheric activity) are long-lived in M dwarfs and the presence of that signature does not necessarily mean the star is young – particularly, most forms of stellar activity can also be induced by magnetic interactions with a close binary. Our analysis must therefore use multiple independent lines of evidence to identify young stars, similar to recent efforts by (Shkolnik et al. 2009, 2012).

The key to our present analysis is trigonometric parallaxes: With parallaxes, we have significantly improved constraints on the kinematics of the systems, AND (along with our photometry) we can use the positions of the constituent stars on an HR diagram with confidence to determine if a system falls along a particular association's isochrones. With our low resolution spectroscopic data, we can measure spectroscopic features sensitive to surface gravity. We can also measure activity features, though the latter are less useful indicators for M dwarfs.

[a] Visiting Astronomer, Cerro Tololo Inter-American Observatory. CTIO is operated by AURA, Inc. under contract to the National Science Foundation.

[1] http://www.recons.org

In section 2, we discuss the sample selection. In section 3, we discuss the observations and reductions of the data in this paper. Section 4 describes the methods we used to determine the ages and association memberships of these objects, and in section 5 we discuss the outcome of the youth analysis carried out on our stars.

This is the thirteenth paper publishing parallax results from the ongoing CTIOPI program[2] at the CTIO 0.9m telescope.

2. The Sample

The sample of 45 star systems in this paper was drawn from the hundreds of targets in the CTIOPI parallax target list. CTIOPI, by virtue of its location, is limited to objects at declinations south of +30 degrees. By using the Tektronix imager at the CTIO 0.9m telescope, CTIOPI is further limited to stars between 9^{th} and 18^{th} magnitudes in at least one of our three Johnson-Kron-Cousins VRI filters. CTIOPI generally targets M dwarf stars whose estimated distances – either from literature, or from our own photometric distance estimates (Hambly et al. 2004; Henry et al. 2004) – place them within 25 pc of the Sun. The targets in this paper are consequently all nearby bright M dwarfs (see Table 2, Column 16).

From the CTIOPI target list, we identified potentially young stars using X-ray saturation ($\log \frac{L_X}{L_{bol}} > -3.5$) as an indicator of chromospheric activity, and overluminosity – herein defined as being more than one magnitude brighter than a single main-sequence star of comparable colors – as an indicator of low surface gravity. As shown by Zuckerman & Song (2004), X-ray emission in M dwarfs is saturated and remains at the $\log \frac{L_X}{L_{bol}} \approx -3.0$ level in stars at least as old as the Hyades (600 Myr), the oldest of the associations we consider here. Therefore, the presence of saturation-level X-ray emission is an excellent indicator (though not guarantor) of youth.

Accordingly, X-ray photometry was obtained from the ROSAT All-Sky Survey (RASS; Voges et al. 1999, 2000) for every available star on the CTIOPI parallax program; the resulting systems have X-ray detections with better than 25% errors on the counts and are within 25″ (95% detection radius, Voges et al. 1999) of the proper-motion-corrected epoch 1991, equinox J2000 coordinates (close to the mean epoch of RASS). The calculation of $\log \frac{L_X}{L_{bol}}$ is taken from Schmitt et al. (1995), using bolometric calculations from Casagrande et al. (2008). We found positive evidence of saturated X-ray emission for 39 of our star systems, many of which are also overluminous.

The remaining six star systems came to our attention purely by the overluminosiy criterion. They exhibit no X-ray emission in the ROSAT catalogs, but their luminosity makes it difficult to explain them as unresolved binaries or triples. (Figure 1).

Among the 45 systems considered here, we have individual photometry and astrometry of 51 components[3], because six of our star systems contain binaries with separations more than 1 arcsecond. Many of the stars in this paper were originally identified as active by Riaz et al. (2006), and several have already been identified as young by Zuckerman & Song (2004), Shkolnik et al. (2012) and Malo et al. (2013). Ten systems were published in previous papers in this series; their astrometry and photometry is reprinted from the earlier papers without change.

3. Observations and Reductions

3.1. Photometry

All CTIOPI photometry is conducted with the CTIO 0.9m telescope, initially (1999-2003) under the NOAO Survey Programs grant; later (2003-present) via the SMARTS Consortium. Photometry is conducted in three filters (Tektronix #2 VRI), utilizing only the central quarter ($6.8 \times 6.8'$ FOV, 401 mas pixel^{-1}) of the Tektronics 2048x2046 CCD to minimize distortions for astrometry. These values are then transformed to standard $V_J R_{KC} I_{KC}$[4] (hereafter without subscripts) photometry using observations of standards from Graham (1982), Landolt (1992), and

[2] A complete table of all published parallaxes is available here: http://www.recons.org/

[3] As seen in Tables 2 and 3, GJ 2022AC was observed for standard photometry but not astrometry, and GJ 799B has resolved astrometry but not photometry

[4] Subscripts: "J" indicates Johnson, and "KC" indicates Kron-Cousins (SAAO system), which is more often known as Cousins. The central wavelengths for V_J, R_{KC}, and I_{KC} are 5475, 6425, and 8075 Å, respectively.

Landolt (2007). The resulting photometry can be found in Table 2. Further details of the observation and reduction procedures can be found in Jao et al. (2005) and Winters et al. (2011). The photometric errors quoted in Columns 3, 4, and 5 of Table 2 combine the Poisson errors, errors on the nightly calibration fit, and standard deviation of multiple nights of photometry (see Column 6). Generally, the latter is the greatest contributor to the collective error, particularly when the star is active, as these stars are. This VRI photometry, along with 2MASS JHK photometry (Cutri et al. 2003), is printed in Columns 11, 12, and 13. The measured colors were used to estimate absolute K magnitudes based on the 12 color-magnitude relations presented by Henry et al. (2004). The photometric distances presented in Column 16 of Table 2 were derived from the mean of the distance moduli implied by the absolute K magnitudes and the 2MASS apparent K magnitude.

Relative photometry (for variability studies) comes from our parallax pipeline. With multiple nights of data in the filter used for parallax, we use the methods in Honeycutt (1992) to derive the nightly offsets and zero points for relative instrumental photometry (Jao et al. 2008) to derive stellar variability. These values are given in Column 8 of Table 2.

3.2. Astrometry

CTIOPI astrometry is carried out using the same telescope and camera configuration as that used for photometry (§3.1) but uses only one filter for each object, chosen to provide the best balance between target(s) and reference star signal-to-noise ratio values. The astrometric pipeline uses all available images taken at hour angles less than two hours, and produces parallaxes, proper motions, and time-series photometry in the parallax filter, all relative to between 5 and 15 "reference" stars within a few arcminutes of the target stars and visible in our images. Parallaxes were corrected to absolute values (Columns 11 and 12 of Table 3) using the mean of the photometric distances to the reference stars, with a typical correction of 1.5±0.5 mas. For a small number of targets with seemingly nearby reference fields (mean photometric parallax esimate, > 3.0 mas), we assume the reference stars are actually reddened by some galactic source, and instead apply the typical correction stated above. Between 2005 Mar and 2009 Sep, a different V-band filter was used for astrometric and photometric observations. While photometrically identical to the original V filter, it exhibited slightly inferior astrometric performance (Riedel et al. 2010), and all astrometric solutions that incorporate data from it are marked as such in Column 16 of Table 3. Additional details of CTIOPI observing procedures can be found in Jao et al. (2005), Henry et al. (2006), and other papers in this series.

3.3. Interferometry

Four of the objects in this paper – BD-21°1074BC, SCR 0613-2742AB, L 449-1AB, and SCR 2010-2801AB – were selected for their X-ray brightness and observed with the Hubble Space Telescope's Fine Guidance Sensors in Cycle 16B, in proposal 11943/11944 ("Binaries at the Extremes of the H-R Diagram") using the F583W filter[5] with no pupil. Reductions were carried out for both axes, providing sub-milliarcsecond precision separations, and delta magnitudes (hereafter Δmag). All four targets were found to be binaries (see § 5.1 below) and their separations, position angles, and magnitude differences were determined by fitting with single-star fringe scans as described by Nelan et al. (2004).

Hubble's Fine Guidance Sensors (FGS) are implemented as three movable units equipped with Koesters prisms, which allow them to function as a 2D interferometer. Two FGS units lock on guide stars and stabilize the spacecraft, while the third (FGS 1r) scans back and forth across the star. Rather than a Michelson interferometer, light is channelled through a linear polarizing beamsplitter, and then through the unit's Koesters prisms, where the light interferes with itself, allowing two dimensions of fringes to be read out simultaneously.

As an interferometric instrument, FGS is capable of measuring single-axis separations as small as 8 mas, for objects as faint as V=16.8. It has been routinely used for orbital mapping and sub-milliarcsecond parallaxes (e.g. Franz et al. 1998; Benedict et al. 1999; McArthur et al. 2011).

[5]The bandpass of the F583W filter is shown here: http://www.stsci.edu/hst/fgs/design/filters (checked 2013 Jun 04)

3.4. Spectroscopy

3.4.1. CTIO 1.5m RCSpec

Spectroscopic observations of all the resolved objects in this paper (except SCR 0613-2742AB) were carried out between 2003–2006 and 2009–2011 using the CTIO 1.5m telescope under the aegis of the SMARTS Consortium. The CTIO 1.5m Richey-Chretien Spectrograph (RCSpec) was used with the 32/I grating setting, covering 6000–9600Å at a resolution of 8Å. Two spectra of each target were taken back-to-back to allow cosmic ray rejection. Data were reduced with standard IRAF techniques using one flux standard per night for absolute flux calibration. No telluric standards were observed, as the data were not originally intended for any purpose other than determining spectral types.

Spectral types were determined by direct comparison to previously obtained standard stars (Henry et al. 2002) spectra. The spectra were prepared by interpolating them onto a fixed 1Å grid running from 6000–9000Å. We then removed telluric features (defined as any region with $> 4\%$ absorption from the Hinkle et al. (2003) sky absorption atlas) and Hα. The target spectra were then compared to the standards by dividing target by standard after cropping both spectra to only the wavelengths where both spectra overlap. The lowest standard deviation $stddev\left(\frac{target}{standard}\right)$ was taken as the best-matching spectral type. The resulting spectral types are presented in Column 14 of Table 2, and have ± 0.5 type errors. Offsets compared to other spectral typing methods (Reid et al. 1995) are of similar size.

Spectral line equivalent widths and indices were computed with the same program, utilizing 11Å windows centered on the maximum or minimum of the feature for both Hα and K I 7699Å. Full bins of 24Å were used for the Na I doublet index. These features were measured prior to removing the telluric and Hα features.

3.4.2. CTIO 4.0m RCSpec

We obtained spectra of SCR 0613-2742AB with the CTIO 4.0m telescope's RCSpec on 2008 Sep 18 and 2008 Sep 19 using the KPGLF-1 (632 g/mm) grating, which covers 4900–8050Å at a resolution of 1.9Å per pixel. The spectral type, Hα, and K I EW measurements of SCR 0613-2742AB come from spectra taken at this telescope, and were calibrated using the same program that analyzed the above CTIO 1.5m RCSpec data.

3.4.3. MPG 2.2m FEROS

One spectrum of SCR 0613-2742AB was taken with the FEROS spectrograph (Kaufer et al. 1999) on the MPG 2.2m telescope at La Silla Observatory on 2013 Feb 18 as part of ESO program 090.C-0200(A). FEROS is an echelle spectrograph fed by two 2.0″ fibers and provides R$\sim$48,000 spectra over a wavelength range of 3500–9200Å. Observations were taken in the Object-Sky mode with the use of the atmospheric dispersion corrector. The data were reduced with the facility pipeline and the IRAF task *fxcor* was used to cross-correlate the target spectrum with several radial velocity standards observed in the same fashion. We measure a heliocentric radial velocity of $+22.54\pm1.16$ km s^{-1} for SCR 0613-2742AB (Table 4). The Na I gravity index measurement and Li 6708Å EW for SCR 0613-2742AB were also derived from these spectra.

3.4.4. CFHT ESPaDOnS

SCR 1425-4113AB was observed on the Canada-France-Hawaii Telescope (CFHT) with the ESPaDOnS (Donati et al. 2006). ESPaDONs was used in the "star+sky" mode, to get a resolving power of R=68000 covering 3700–10500Å over 40 grating orders. The data were reduced by the queue service observing team using UPENA pipeline. We measure a heliocentric radial velocity, lithium EW, and $v \sin i$ for both targets in the system.

4. An Assessment of Stellar Youth Tracers

Our available data – trigonometric parallaxes, low resolution red optical spectroscopy, and $VRIJHK$ photometry for the entire sample – provides four methods of young star identification at our disposal: UVWXYZ Kinematics, Isochrones, the Bayesian Analysis for Nearby Young AssociatioNs (BANYAN) statistical method, and gravity sensitive features. Taken individually, none offers conclusive proof of youth. Together, they present a strong case for the youth (and specific association membership) of the systems described here.

The measured data used to make our conclusions are given in Table 4, Table 5, and Table 6; the results of our analysis are given in Table 7.

4.1. UVWXYZ Kinematics

Stars that form together should be moving together through space. Over time, internal and external interactions will cause them to disperse into the thin disk of the Galaxy. The associations we consider here (Table 8) are all sufficiently young that this has not happened yet, even though (with the exception of η Chameleontis, the Pleiades, and the Hyades) they are gravitationally unbound.

The perhaps hundreds of systems in an association are spread out over tens of thousands of cubic parsecs, interspersed among thousands of field systems (and, indeed, members of other young moving groups), and as an unbound association, their velocity dispersions are larger than 1 km s^{-1}. Therefore, large numbers of older stars (López-Santiago et al. 2009 in particular quotes $\sim 30\%$) will coincidentally happen to have matching UVW motions, and even larger numbers of field stars will fall within the spatial boundaries of an association. UVW motions do not prove youth, but they are necessary to connect young stars to young associations.

There is also the non-trivial issue of whether we have an accurate assemblage of these nearby associations and moving groups. We adopt the associations in Table 8 despite the knowledge that the physical reality of these groups (and the accuracy of their proposed members) is still somewhat uncertain. For instance, the IC 2391 Supercluster (Eggen 1991), Carina-Vela moving group (Makarov & Urban 2000), and Argus association (Torres et al. 2008) have all been proposed as the extended halo of the nearby IC 2391 open cluster, but all are more or less distinct from each other in terms of membership and proposed properties; currently only Argus is thought to be an actual co-eval assembly.

4.1.1. The Kinematic Data

Computing UVWXYZ kinematics requires requires R.A., Decl., π, $\mu_{R.A.\cos Decl.}$, $\mu_{Decl.}$, and radial velocities for UVW velocities; and R.A., Decl., and π for XYZ positions. The input data used for this analysis (presented in Table 4) differs in several key ways from the pure CTIOPI astrometric data in Table 3:

For most star systems, the only available spectra are from the CTIO 1.5m RCSpec, which lacks the resolution necessary for radial velocities. We have obtained radial velocities from the literature to fill out our sample.

We use weighted mean parallaxes for systems that have multiple reported parallaxes – either from multiple system components, or parallax determinations from other parallax programs. In doing so, we have made two key assumptions: That all components of a star system are at the same effective distance to currently achievable accuracy; and that all published parallaxes are reasonably free of systematics.

The CTIOPI pipeline produces relative proper motions (as shown in Table 3) by assuming each target field's astrometric reference stars have no net motion, which is not strictly true. In order to have unbiased results, we ideally want to use absolute proper motions for our kinematic determinations. Comparing our results to the absolute International Celestial Reference System (ICRS) proper motions[6] from UCAC4 (Zacharias et al. 2013), we find mean offsets of $+5.12 \pm 12.80$ mas yr^{-1} in $\mu_{R.A.\cos Decl.}$ and -0.78 ± 9.45 mas yr^{-1} in $\mu_{Decl.}$, uncorrelated across the sky. The small differences but large uncertainties suggest CTIOPI proper motions are accurate relative to the UCAC4 ICRS grid, but the uncertainties are undersampled. Where possible, we use UCAC4 absolute proper motions directly. Where no UCAC4 proper motions are available, we use our proper motions, with the above offsets added in as a systematic uncertainty. In two cases – L 449-1AB and AP Col – the UCAC4 proper motion was discrepant with the CTIOPI proper motion by more than 100 mas yr^{-1}, and we used the CTIOPI proper motion with the uncertainty.

4.1.2. The Kinematic Method

The standard method for computing UVW space velocities is laid out in Johnson & Soderblom (1987), and the matricies in that paper can eas-

[6]Note that UCAC4 also includes high proper motion objects from relative proper motion sources, including previous CTIOPI papers. Such entries are identifiable by flags within the database.

ily be adapted to compute XYZ space positions. These UVWXYZ coordinates are right-handed Cartesian Galactic coordinates aligned so that the U/X axis is toward the galactic center, the V/Y axis is in the direction of galactic rotation, and the W/Z axis is toward the North Galactic Pole. In cases where we have full kinematic information, we calculate 10^7 Monte Carlo iterations to fully sample the uncertainties on our input kinematics as a three-dimensional ellipsoid in velocity space. For stars without radial velocity measurements, we calculate 10^5 Monte Carlo iterations at multiple different radial velocities within a range -100 to $+100$ km s^{-1}.

To determine whether a star system is a potential match for a given association, we must determine how close the three-dimensional velocity-space ellipsoid(s) defined by our Monte Carlo iterations is to the three-dimensional velocity-space ellipsoid of the association, as defined in Table 8. Because the dispersions are meaningful – in the case of the sample system, they represent the uncertainty on the velocity of the system; in the case of the association, they represent the intrinsic dispersion of real members – our phase-space "separations" are calculated relative to those dispersions, in the form of our goodness-of-fit statistic γ:

$$\gamma = \frac{1}{3}\left(\frac{(U_{assoc}-U_{system})^2}{(\sigma^2_{U_{assoc}}+\sigma^2_{U_{system}})}+\frac{(V_{assoc}-V_{system})^2}{(\sigma^2_{V_{assoc}}+\sigma^2_{V_{system}})}+\frac{(W_{assoc}-W_{system})^2}{(\sigma^2_{W_{assoc}}+\sigma^2_{W_{system}})}\right) \quad (1)$$

This γ statistic is effectively identical to the one used in Shkolnik et al. (2012), where it appears as $\bar{\chi}^2$.

We take a value of γ less than 4 as a potentially significant match. In many cases, a system will be kinematically consistent with membership in more than one young association. This is often unavoidable, as the velocity distributions of several associations genuinely overlap; in these cases we must look at the other diagnostics to determine which association is the most consistent with the available data. In cases where we have no radial velocity, we fit the resulting γ values from our range of points to determine a best-fit radial velocity and γ. Only the γ value for the most consistent association is given in Column 5 of Table 7.

4.2. Isochrones

Pre-main-sequence stars are still in the process of contracting under gravity, and are still physically larger than main-sequence stars of the same temperature, and consequently much brighter. It is therefore possible to distinguish stars of a given age using isochrones, or at least demonstrate the youth of a system.

4.2.1. The Photometric Data

Overluminosity is also a sign of multiplicity, and must therefore be taken into account before making conclusions about the potential youth of a system based on its luminosity. Our sample has many multiple stars (See Table 10), which are not resolved in CTIOPI images if they are less than $\sim 2''$ apart. In order to properly distinguish between binaries (which in the maximal case of an equal-luminosity pair can be 0.7 mag brighter than a single star) and young stars, we have made an extensive literature search for multiples within the sample. Once multiples are identified, their photometry must be de-blended to properly place them on a color-magnitude diagram.

Unfortunately, we do not have both ΔV and ΔK_S values for any multiples in our sample, so the deblending in one of the filters must be estimated. Plotting, for instance, M_V vs M_{K_S} (Figure 4) demonstrates that the relation is, to a first approximation, linear between M_V=1 and M_V=15 (M_{K_S}=1 and M_{K_S}=9), in that case with a slope of 1.8, for $\Delta V = 1.8 \times \Delta K_S$. We list all the equivalencies in Table 11. Actual measurements should definitely be preferred, however, as the error on the fit slopes are on the order of 0.03, and the residuals to the fits are on the order of 0.5.

For purposes of deblending our stars, we have assumed that the $\Delta FGS583W$ values are equivalent to Kron-Cousins ΔR, and that all the various ΔK values (CIT, Altair, MKO, 2MASS) are equivalent to 2MASS ΔK_S. Several systems are known only as spectroscopic binaries. With no other information available, we have assumed $\Delta V = \Delta K_S = 0$. The photometric data used in the isochrone analysis, including deblended magnitudes, are given in Table 5 and used to place stars on the Color-magnitude diagram in Figure 3. Deblended optical magnitudes are given for the brown dwarfs TWA 27B and SCR 0103-5515C, but

their deblended V magnitudes are suspect at best.

4.2.2. The Photometric Method

Because isochrones do not match field main sequence stars well at low masses (Hillenbrand & White 2004), we are using empirical "isochrones" from Riedel et al. (2011), which are empirical polynomial fits derived from known young stars with photometry and trigonometric parallaxes, for the four associations – TW Hya, β Pic, Tuc-Hor, and AB Dor – with a sufficient number of known low-mass members to make the isochrones useful. Plotting our stars on color-magnitude diagrams with these isochrones (Figure 3) demonstrates that many are indeed overluminous relative to main sequence stars. Note that several stars (SCR 0103-5515C, LP 655-48, TWA 27A and B) are too red and faint to appear in the figures, and the Tuc-Hor isochrone line from Riedel et al. (2011) does not extend into the M dwarfs shown due to lack of data.

4.3. BANYAN

BANYAN (Malo et al. 2013) is an independent Bayesian methodology for finding young stars. BANYAN uses IJ photometry, Baraffe et al. (1998, 2002) model isochrones, and a slightly different set of UVWXYZ values for the known associations. It searches for members of the known nearby associations β Pictoris, TW Hydra, Tucana-Horologium, Columba, Carina, Argus, and AB Doradus, with "Field" as the default hypothesis. It is presented as a complementary, proven method. The coefficients for the best-matching association are shown in Table 7, Columns 5 and 6.

4.4. Low Surface Gravity

Three gravity-sensitive features exist within the 6000Å–9000Å coverage of our spectra: Ca II (8498,8542,8662Å) is strong in giants and weak in dwarfs; Na I (8183,8195Å) and K I (7665,7699Å) are weak in giants and strong in dwarfs. The general pattern is that the neutral alkali and alkali earth metals are increasingly strong with higher gravity, while their singly ionized variants grow weaker with higher gravity (Allers et al. 2007; Schlieder et al. 2012a).

In this paper we are using the Na I index as defined in Lyo et al. (2004a), and the K I 7699Å doublet line (the other is contaminated by the atmospheric A band). The Na I index value is formed by the ratio of the average flux in two 24 Å wide bands:

$$NaI_{index} = \frac{F_{8148-8172}}{F_{8176-8200}} \quad (2)$$

Measurements for the program stars are given in Table 6, and graphs of the general trends are shown in Figure 5. Unfortunately, as can be seen in the figures, young stars and main-sequence stars overlap at colors bluer than $V - K_s = 5$, in both cases. The lines can also be affected by stellar activity, where emission fills in the absorption line cores, leading to lower EWs (Reid & Hawley 1999).

In principle, multiplicity and metallicity will have an effect on these features. The effects are muted in the case of multiplicity, as the brighter component will dominate, and the line will not be appreciably weaker or stronger than that of a main-sequence star of the same color. Metallicity is more difficult. While we can expect low-metallicity subdwarfs to have weaker lines due to lower abundances, subdwarfs plot *below* the main sequence and will not be mistaken for pre-main-sequence stars. However, as noted by Shkolnik et al. (2009), high metallicity stars of a given mass and bolometric luminosity will masquerade as stars of lower temperature *and* lower surface gravity. The additional metals increase the opacity of the stellar atmosphere and therefore put the effective photosphere farther from the center of the star. Thus, these stars will appear above the main sequence – in fact, these gravity-sensitive atomic species are the ones used by Rojas-Ayala et al. (2010) to measure the metallicity of field M dwarfs.

With the exception of SCR 0613-2742AB and SCR 1425-4113AB, the only available spectra for the sample stars are low resolution flux-calibrated optical spectra from the CTIO 1.5m telescope that cannot be reliably corrected for telluric absorption. Thus, there is an additional source of error in our Na I index measurements, and we are using only one of the K I doublet lines (the other is within the atmospheric A band). We conclude that while we see some indication of offsets for young stars in the plots of Figure 5, conclusions of

youth using this method with data at this resolution are only tentative.

4.5. Activity-based features

4.5.1. X-ray activity

As seen in Zuckerman & Song (2004), X-ray activity remains saturated in M dwarfs even beyond 600 Myr. Consequently, X-ray activity is a considered as a necessary but insufficient marker of a star system's youth, and its presence was mostly useful in our sample selection process.

There are, however, eight objects in our sample without X-ray emission. These objects comprise the six previously mentioned systems with no X-ray emission, and two components (GJ 2022B and LP993-115A) of systems with other X-ray detected components. For those targets, we calculate upper limits on their X-ray emission (see Table 6, Columns 4 and 5) using the cnts s^{-1} $arcmin^2$ for the nearest target in the RASS catalog (generally under $2'$ distant) as the local background countrate. Even assuming a hypothetical one-arcminute point spread function, of the eight objects, only TWA 27AB can potentially have saturated X-ray emission, unless the background count rates for ROSAT are remarkably different over small angular separations. For the special case of NLTT 372, G 131-26AB is also within the $25''$ radius we used to localize X-ray detections. Although the emission is more likely associated with G 131-26AB, if the observed X-ray counts are actually being produced by NLTT 372, it would be one of the most coronally active stars in our sample.

ROSAT's resolution and accuracy cannot spatially distinguish between targets that are within $\sim 25''$ of each other. Consequently, there are a few cases where a multiple system is resolved in the optical and near-infrared but not in X-rays. In these cases, we have *combined* the V and K_S photometry to produce a system bolometric flux. We did not blend NLTT 372 and G 131-26AB, because despite being arcseconds from each other, they are two separate star systems.

4.5.2. Hα emission

M dwarfs also have saturated Hα emission for long periods of time (West et al. 2008). We have measured this value (Table 6), but it cannot be used to distinguish between the ages of low-mass pre-main-sequence stars. The only useful purpose of Hα emission for low mass stars is to provide an upper (if present) or lower (if absent) limit on ages, which has been done in done in Table 7 following the prescription in West et al. (2008). Though we see substantial Hα emission in a few of our stars, none of their emissions reach the White & Basri (2003) threshold necessary to be considered a T Tauri star (see Figure 6).

4.5.3. Photometric Variability and Flares

One of the hallmarks of the T Tauri class of young stars is variability, and this extends into the older non-accreting stars discussed here. Analysis of the relative variability of M dwarfs (Jao et al. 2011) shows that a typical M dwarf varies by roughly 0.010 magnitudes, and statistically significantly more in V and R (0.013 mag) than I (0.008 mag). They also found a statistically significant difference between regular M dwarfs and their older, metal poor subdwarf cousins (variability 0.007 mag, our observational "floor") which points to some combination of age and (possibly) metallicity influencing the amplitude of stellar variability. As seen in Figure 7, M dwarfs with variability higher than 0.020 mag are rare, although many are present among the young stars in this paper.

While many stars in this paper are known flare stars or UV Ceti variables, only two stars were seen to flare during the course of astrometric observations: TWA 8B and GJ 1207. The relative photometry during the flares is reproduced in Figure 8.

5. Candidate New Association Members

Of the 45 systems in this paper, 25 have their first trigonometric parallaxes published here. 15 of the 45 systems (including LP 476-207=HIP 23418) are now new members of the sample of all stars with trigonometric parallax distances within 25 pc.

Seven systems are known triples (including GJ 799AB = AT Mic, whose primary is the star GJ 803 = AU Mic) and 13 are known binaries (Table 10). 25 systems are currently not known to be multiple, though four (NLTT 372, SCR 0757-7114, LEHPM2-0783, SCR 2033-2556) are strongly sus-

pected to be multiple based on our youth analysis, and one (SCR 0103-5515ABC) seems to be too bright even when its multiplicity is taken into account. Thus, these 45 systems include at least 72 objects, for a companion fraction (companion stars/systems) of 60% and a multiplicity fraction (multiple systems/single systems) of 47%, similar to what was reported by Fischer & Marcy (1992) for a collection of M0–M3 dwarfs. This high multiplicity rate is to be expected, considering that luminosity (the result of youth or multiplicity) was a defining characteristic of the selection process.

We find 21 potential and/or confirmed members of nearby young associations (Table 7, Column 10). Within the sample, we recover ten members of β Pictoris, four members of TW Hydra, two members of Argus, two members of AB Dor, and two young members of unknown associations. In addition, there is one system kinematically consistent with the Ursa Majoris moving group, although by gravity and HR diagram position it is not distinguishable from a main sequence star. Particularly noteworthy are the seven new members of β Pictoris. Several systems are potentially kinematically consistent with the Hyades, but as all are more than two tidal radii (10 pc) from the Hyades, and the existence of the Hyades Stream has been brought into question by Famaey et al. (2008), we suspect all potential Hyades embership are not physical (see §5.1).

Several of our objects are likely cooler than the threshold where M dwarfs become fully convective (around $V - K = 5.8$), and at least three (SCR 0103-5515C, TWA 27A, TWA 27B) are brown dwarfs. It is difficult to make comparative conclusions about such systems, as very few comparably low-mass systems are known in these associations.

For AB Dor, Ursa Major, and Castor, our analysis is more tentative, given that members of those systems are difficult to distinguish from main sequence stars using isochrones and gravity-sensitive lines, leaving us with only the kinematic analysis. Confirmation of membership in these associations will require measurements of the stars' radial velocities, lithium, chemical abundances (Castro et al. 1999; Barenfeld et al. 2013), and (in the case of Castor) further study to determine if the moving group genuinely exists at all (Mamajek et al. 2013).

5.1. Notable Systems

(in order of Right Ascension)

NLTT 372 was originally part of the reference field of the system G 131-26AB. It is within the error circle of the ROSAT X-ray source we attribute to G 131-26AB, and may either contribute or be the source of those X-rays. It is more luminous than a single star of its photometric colors, and is likely to be a binary.

GJ 2006AB appear to be β Pictoris members, based on kinematics, gravity, and their positions relative to the β Pictoris isochrone. A spectrum of GJ 2006A was obtained with VLT instrumentation (Malo et al. in preparation) and the radial velocity was determined to be +8.90 km s^{-1} with $v \sin i$ of 6 km s^{-1}, in excellent agreement with that of a predicted β Pictoris member.

SCR 0103-5515ABC was resolved as a close triple by Delorme et al. (2013) composed of two M dwarfs, A and B, and a more spatially distant brown dwarf, C (see Table 10). Delorme et al. (2013) and the BANYAN results find it to be a match to Tucana-Horologium, but we find that its kinematics better match the Carina association, and because both associations are supposed to be the same age, we cannot distinguish between them with the other methods. When their photometry is deblended, both components lie *above* the β Pictoris isochrone, implying that they are younger than β Pic, even though Tucana-Horologium and Carina are both supposed to be older than β Pic. The system is undoubtedly young, but more observations are needed to determine if it is a higher-order multiple in Tuc-Hor, or something entirely different.

GJ 2022ABC is a hierarchical triple (see Table 10) composed of a wide (37.8″) companion (B) to a close (1.8″) nearly-equal-luminosity pair (AC) with a delta magnitude of roughly ΔV=0.08 (Jao et al. 2003; Daemgen et al. 2007). The B component is actually the least luminous, though to preserve the historical order of discovery, we continue to refer to it as 'B'. The AC component is bright in RASS; there is no corresponding detection of the B component.

The A and C components are separated by 1.8″ (Figure 9). They are separable and (as they are much brighter than the B component) unsaturated on only 31 of the 66 images taken. Those

31 images were taken on 14 nights spanning 11.89 years and positions were obtained using special extra-sensitive (but less precise) SExtractor settings. A reduction of all three components yields

- GJ 2022A: π =40.91±5.64 mas, μ =210.5±1.3 mas yr^{-1} @ 126.5±0.71°
- GJ 2022B: π =42.12±3.60 mas, μ =206.2±0.8 mas yr^{-1} @ 127.4±0.46°
- GJ 2022C: π =46.96±5.31 mas, μ =200.6±1.2 mas yr^{-1} @ 126.8±0.71°

This implies a weighted mean parallax of 43.05±2.63 mas (23.2±1.4 pc), which is consistent with our main reduction of B in Table 3 using 66 frames (38.80±2.13 mas, 25.8±1.4 pc) and with membership in the AB Dor association. Formally, we are using the parallax of the B component alone as our system parallax in Table 4 due to the lower precision of the results for all three components.

LHS 1302 is potentially a kinematic match for the ∼30 Myr old Columba association, but its gravity (Figure 5) and isochrones (Figure 3) suggest it is a field object.

LP 993-115 (A)/LP 993-116AB (BC) We detect the astrometric orbital motion of the BC pair (Figure 10). Our attempt to fit an orbit did not converge, and the astrometry in Table 3 was calculated without compensating for orbital motion. This triple system appears to be composed of field stars, and only the BC components have X-ray emission.

LP 476-207ABC was observed by *HIPPARCOS* as HIP 23418; the resulting parallax was of poor quality due to erroneous coordinates in the input catalog (Perryman et al. 1997) and the resulting poor available astrometry. Our new result (24.6±1.3 pc) is significantly closer and higher precision than the old (Perryman et al. 1997) (32.1±8.8 pc) and revised (van Leeuwen 2007) (33.2±10.5 pc) *HIPPARCOS* values, but the system is still in β Pic.

BD-21°1074ABC is a known member of the β Pic association (Torres et al. 2008; Malo et al. 2013). The A component was not originally targeted for parallax measurement and was saturated in many early images; the parallax result in Table 3 is of lower precision.

The BC component was observed by the Hubble Space Telescope Fine Guidance Sensor Interferometer on 2008 Dec 18, and resolved (Figure 12) in both axes, with details in Table 10. The measured position angle is discrepant with the current Washington Double Star catalog value (0.8″ @ 321°) but matches the angle of the visible elongation of the BC point spread function from CTIOPI data, as seen in Figure 13. We see an astrometric binary signal in our astrometry, as shown in Figure 11

L 449-1AB was identified as an active star by Scholz et al. (2005). This system was on the HST Cycle 16B FGS proposal, and was resolved into two stars on 2008 Dec 03 (Figure 14) with $\Delta F583W = 0.95$ mag (see Table 10). By HR diagram isochrones and gravity indices, this system is indistinguishable from main sequence stars. The system's kinematics are a potential match for the Ursa Major moving group, which given the probable age of 500 Myr (King et al. 2003) again suggests that the components may be nearly Zero-Age Main Sequence (ZAMS).

LHS 1358 has kinematics consistent wih the Hyades stream. Various authorities (e.g. Famaey et al. 2008) dispute the existence of the stream as a real kinematic entity; at only 15.3±0.5 pc from the Sun, LHS 1358 is a minimum of 30 pc (3 tidal radii) from the Hyades cluster center, and therefore the identification is not physical.

SCR 0613-2742AB is the lowest proper motion system (11.2±1.0 mas yr^{-1}) thus far observed on CTIOPI, with a transverse velocity of 1.6 km s^{-1}. The system is a binary, observed on 2008 Dec 4 and resolved into two stars (Figure 16, Table 10) by FGS, and is also detected as a binary by our FEROS spectroscopy. We see orbital motion in the CTIOPI astrometric residuals of this star (Figure 17) and have removed that orbital motion[7] from our astrometric results (Riedel et al. 2010), but we do not have data on a full orbit. Based on the FEROS spectroscopy, we see no Li 6708Å doublet absorption. This is expected for β Pictoris members near the Lithium Depletion Boundary

[7]The orbit that was fit assumes a 4.67 year orbit starting at T_0 of 2010.803 Julian Years, with photometric semimajor axis 0.54 arcsec, inclination 89.9 degrees, eccentricity of 0.9999, a longitude of the ascending node of 201.3 degrees, and longitude of periastron of 90.3 degrees. While it removes the orbital bias from our astrometric data, we do not consider the orbit correct.

(Yee & Jensen 2010).

The position and proper motion of SCR 0613-2742AB, near the convergent point of the β Pic association, are extremely similar to those of 2MASS J06085283–2753583 (Cruz et al. 2003; Rice et al. 2010), a brown dwarf β Pic member. The parallax of 2M0608 (32.0±3.6 mas, 31.3±3.5 pc) (Faherty et al. 2012) is also very similar to SCR0613 (34.0±1.0 mas, 29±0.9 pc). The two systems are separated by 3529″ @78.6°, which yields a minimum projected separation of 100 kAU (≈0.5 pc). It is difficult to compare their proper motions – (+8.9,+10.7)±(3.5) mas yr^{-1} relative (2M0608) and (−13.1,−0.3)±(11.6,15.5) mas yr^{-1} absolute (SCR0613) – given the large uncertainties involved, save that each are marginally consistent with both zero and each other.

Meanwhile, the binding energy, $U_g = \frac{-GM_1M_2}{r} = -1.28 \times 10^{33} J$ using the conservative estimates that the two components of SCR0613 have a combined mass of $0.5 M_\odot$, and 2M0608 is $0.015 M_\odot$. This binding energy is lower than any of the extremely wide systems studied in Caballero (2009), and it is probable that these stars are not gravitationally bound. It is possible that this *was* a bound system at one point (like AU/AT Mic=GJ 803/799AB, below), but is not any longer.

SCR 0757-7714 is overluminous by 2 magnitudes, plotting near the β Pic isochrone on the HR diagram in Figure 3, and has low surface gravity based on its K I measurement, but not Na I. Surprisingly, it shows no other signs of youth or membership in any known association – in fact, it has no X-ray emission, and is the only star under consideration with Hα in *absorption*. Thus, the star's elevation on the HR diagram is most likely due to unresolved multiplicity.

L 34-26 is a potential kinematic match to the Ursa Major moving group, but its measured radial velocity (+0.9 km s^{-1}, no error, Torres et al. 2006) is most likely discrepant with the best-fit Ursa Major moving group radial velocity, +6.6 km s^{-1}.

SCR 1012-3124AB is a close ∼1″ binary (Figure 18, Table 10). There are a few epochs where the B component (to the west of the A component) can be seen, but for the most part the two components are blended in our astrometric observations.

Radial velocity measurements with the VLT-UT1 CRyogenic high-resolution infraRed Echelle Spectrograph (CRIRES) presented in Malo et al. *submitted* confirm the star's multiplicity, and yield radial velocities of 14.69±0.53 km s^{-1} and 14.43±0.75 km s^{-1}, for A and B respectively. The $v \sin i$ measurements (A: 15.52±2.01 km s^{-1}; B: 20.40±2.58 km s^{-1}) are also indicative of youth, where Reiners et al. (2009) considers $v \sin i > 20$ km s^{-1} the minimal condition for a 'fast rotator'.

While it is outside the normal spatial bounds (Torres et al. 2008) of the TW Hydra association (its R.A. is slightly lower than that of TWA 21, at 10h13m), its UVW kinematics are consistent with TW Hydra, as is its deblended isochrone position (Figure 3). Its gravity measurements (Figure 5) indicate it is extremely young.

TWA 8AB was listed by Jao et al. (2003) as RXJ1132-264AB and was not included in the TW Hydra analysis of Weinberger et al. (2013); our information is consistent with their conclusions based on other members of TW Hydra in that analysis.

G 165-8AB appears to be between the ages of β Pictoris and AB Doradus based on its gravity measurement and deblended HR diagram positions. There are two highly discrepant radial velocities published for this system, $+8 \pm 0.1$ km s^{-1}, Montes et al. (2001) and -7.5 ± 6.5 km s^{-1}, Gizis et al. (2002). We would normally choose the former value due to its higher precision, but the kinematics derived using that value agree with no known association. Ignoring radial velocities altogether, we find best-fit matches to to the Tucana-Horologium (γ=0.58, best-fit RV −6.2 km s^{-1}), Carina (γ=0.62, best-fit RV −10.4 km s^{-1}), and Columba (γ=2.40, best-fit RV −12.5 km s^{-1}) associations, all with estimated ages of 30 Myr. It seems likely that the Gizis et al. (2002) radial velocity is accurate, and the uncertainty is accounting for orbital motion of the binary. Using the latter radial velocity, the best match is to Carina, though BANYAN favors Columba.

Unusually, this system is a northern hemisphere target well outside the published spatial boundaries of all three associations. This suggests that either there is a fourth 30 Myr old association nearby, possibly containing two other northern hemisphere objects thought to be members of the 30 Myr old Columba association: HR 8799

(Marois et al. 2008; Baines et al. 2012) and κ And (Carson et al. 2013), or that the existing assumptions about the boundaries of the known associations are incorrect.

SCR 1425-4113AB is a curious system. High resolution ESPaDOnS spectra of this target show that it is a spectroscopic binary, and an extremely rapid rotator ($v \sin i$ = 95.0±8.1 km s^{-1}), with a radial velocity of (−1.2±1.3 km s^{-1}). Its lithium EW was also measured at 595±20 mÅ, confirming its youth. The deblended magnitudes of both of its components place them above (though consistent with) the TW Hydra isochrone on an HR diagram, and the gravity measurements (which should not be affected by multiplicity) place it at lower surface gravity than TWA 8AB and SCR 1012-3124AB (though still within the errors).

Our kinematics find it to be a much better fit to β Pictoris (γ=0.59) than TW Hydra (γ=6.46), but BANYAN finds 75% probability of it being a TW Hydra member, compared with 24% probability that it is actually a β Pictoris member. It is additionally outside the normal spatial boundaries of TW Hydra (being a full hour of R.A. 'higher' than the highest current member, TWA 18, at 13h21m R.A.). We nevertheless consider it as a potential TW Hydra member because with its extremely high luminosity, low surface gravity, and position relatively close to TW Hydra, it either must be an outlying member of TW Hydra or something equally young.

SCR 2010-2801AB was found to be a binary by Bergfors et al. (2010). The system was observed with HST-FGS on 2009 Apr 26, as seen in Figure 19. The resulting separation agrees with the separation published in Bergfors et al. (2010).

LEHPM2-0783 has X-ray emission and the strongest H-α emission in the sample, despite its cool temperatures. It lies above the main sequence, though it is too red to be seen on Figure 3. It is, however, not a potential kinematic match to any known young association. It may be younger than a typical field star, but we have no reason to suspect it is anything more than an unresolved binary.

L 755-19 is kinematically consistent with both Castor and Argus. It lies within the upper main sequence locus, above the AB Doradus isochrone, which would be more consistent with the Argus association (younger than AB Dor) or a main sequence binary than the Castor moving group (older than AB Dor). L 755-19 is a hotter star than AP Col (Riedel et al. 2011), and its surface gravity is comparable with either field stars or Argus-age objects. A radial velocity would go a long way toward determining the status of this star, given that the best-fit Argus RV is −25.4 km s^{-1}, and the best-fit Castor RV is −9.3 km s^{-1}, and a Castor/Main Sequence assignment would imply it is a binary.

SCR 2033-2556 is consistent with being a member of β Pictoris, but its high luminosity suggests it is an unresolved binary. Observations with ESPaDOnS (Malo et al., *in prep*) suggest a lithium equivalent width of 510 mÅ, confirming the star's youth.

GJ 803 (A)/GJ 799AB (BC) is one of the nearest young systems (see Table 10) to the Sun, and a prototypical member of the β Pic association (Barrado y Navascués et al. 1999). AU Mic (unobserved by CTIOPI) is known to have a dust disk, and several authors note that the AU-AT Mic separation is very large (at least 0.23 pc) and "must be very fragile and will soon be torn apart by third bodies" (Caballero 2009). This system is a well-established member of the 10 parsec sample with parallaxes from *HIPPARCOS* and the Yale Parallax Catalog (van Altena et al. 1995); our results agree with the published values.

In our first epoch (2003 JULY 09) GJ 799 A and B were separated by 2.8″ @ 171°; in our final epoch (2012 JULY 31, Figure 20) they were separated by 2.3″ @ 153°.

GJ 1284AB is identified as a potential member of Columba by kinematic analysis; however, Torres et al. (2006) identified it as a spectroscopic binary, which implies it is a system of main-sequence stars, and the kinematic match is spurious.

6. Conclusions

We have identified 21 young systems, of which 14 are new, and six – LP 467-16AB, G 7-34, L 449-1AB, G 165-8AB, L 755-19, and SCR 2033-2556 – are within 25 pc of the Sun, as outlined in Table 6. This constitutes 6% of all known β Pictoris members, and adds two new TW Hydra members that are outside the currently understood boundaries of

the system. We also further increase the number of nearby Argus and AB Doradus members. Additionally, the enormous number of multiples will be enormously beneficial to studies of stellar masses for young stars; there are less than 10 masses for M dwarf stars less than 10 Myr old (Mathieu et al. 2007) and therefore considerable discrepancies in the various predicted evolutionary tracks of low-mass stars; this paper includes three new spectroscopic binaries in TW Hydra and β Pictoris where *every* component is less than $0.5M_{\odot}$.

The most interesting results of this analysis are the contradictions with expected young star behavior. Six systems in the sample are clearly overluminous but none of their components have RASS X-ray detections. Three of them – SCR 0103-5515ABC, SCR 1012-3124AB, and SCR 1425-4113AB – show Hα emission in low-resolution optical spectra; all three are definite young systems, and all three are multiples. The fourth target, SCR 0757-7114, shows no signs of activity at all and is more likely a triple or quadruple system. The remaining two objects – NLTT 372 and TWA 27AB – were not observed spectroscopically, so we cannot comment on their Hα EW (though Gizis & Bharat (2004) recounts wildly varying Hα emission from TWA 27AB).

We checked the XMM-Newton and Chandra observing logs to see if any of the six systems were observed by higher-sensitivity equipment, and found a Chandra observation of TWA 27AB. That observation formed the basis of the work by Gizis & Bharat (2004), who report no detected X-ray flux in a 50 ksec observation, and provided only an upper limit. Given that TWA 27AB was the only target that might have had saturated X-rays given the upper limit from RASS photometry, we can fairly conclusively state that none of these systems exhibit X-ray emission.

It is not clear how these six systems (or GJ 2022B and LP 993-115) exhibit such low X-ray activity at such young ages, except to point out that Hα emission is thought to be produced in the chromosphere, and X-ray activity originates in the corona; Riaz et al. (2006) and West & Basri (2009) have noted that Hα emission does not correlate well with X-ray activity. Gizis & Bharat (2004) suggest the enormous (and variable) Hα emission they have compiled from TWA 27AB, combined with its lack of X-ray activity, implies that the corona and chromosphere are quiet, and the Hα activity actually comes from accretion. Given that SCR 1012-3124AB and SCR 1425-4113AB are both suspected members of the same 8 Myr old TW Hydra association, it is not inconceivable for them to have disks, though more observations will be needed. Explaining a disk around SCR 0103-5515ABC is more difficult, considering that as a member of Tucanae-Horologium it is expected to be $\sim$30 Myr old, though with its high luminosity for the two stellar components, we do have evidence that it may be a younger system.

The issue of X-ray emission highlights the reason why we favor a checklist-style or multi-parameter approach to youth, such as those used by Shkolnik et al. (2009, 2011). None of the indicators of youth are infallible – if we were to strictly require X-ray saturation, we would have missed both new potential TW Hydra members, and have only noticed the AB Doradus member GJ 2022B (Shkolnik et al. 2012) on the strength of its companions – but together they can provide a clearer and more robust picture of youth. Equally important, these stars are variable, and some number of them will be caught by any given survey in a transient inactive state.

We also have a small assortment of stars that do not quite fit into our current knowledge of young clusters: Both of the putative new TW Hydra members (SCR 1012-3124AB and SCR 1425-4113AB) lie outside the spatial bounds of the TW Hydra association members defined in Torres et al. (2008); G 165-8AB is clearly young, but lies outside the spatial and kinematic boundaries of all known suitably young associations. SCR 0103-5515A and B are each too luminous to be members of Tucana-Horologium or Carina unless both are further close multiples. (each lies $\sim$0.4 magnitudes above the β Pictoris isochrone, as do LP 476-207B, SCR 2010-2801A and B, and SCR 0017-6645, though in those cases our deblending method may be at fault, see §4.2.1). Ultimately, further study is needed to determine the true extent of these young associations, and determine what manner of processes have brought the associations to their current state.

The RECONS effort is supported primarily by the National Science Foundation through grants AST 05-07711 and AST 09-08402, and was sup-

ported for a time through NASA's *Space Interferometry Mission*. Observations were initially made possible by NOAO's Survey Program and have continued via the SMARTS Consortium. This research has made use of the SIMBAD database and the VizieR catalogue access tool, operated at CDS, Strasbourg, France; NASA's Astrophysics Data System; the SuperCOSMOS Science Archive, prepared and hosted by the Wide Field Astronomy Unit, Institute for Astronomy, University of Edinburgh, which is funded by the UK Science and Technology Facilities Council; the Washington Double Star Catalog maintained at the U.S. Naval Observatory; and the NStars project. This publication makes use of data products from the Two Micron All Sky Survey, which is a joint project of the University of Massachusetts and the Infrared Processing and Analysis Center/California Institute of Technology, funded by the National Aeronautics and Space Administration and the National Science Foundation, and the AAVSO Photometric All-Sky Survey (APASS), funded by the Robert Martin Ayers Science Fund. This research has made use of the Washington Double Star Catalog maintained at the U.S. Naval Observatory. D.R.R. acknowledges support from project BASAL PFB-06 of CONICYT, a Joint Committee ESO-Government of Chile grant, and FONDECYT grant #3130520. S.C.B and E.L.R acknowledge support from NASA award 11-ADAP11-0169.

The authors also wish to thank Dr. Brian Mason for supplying the orbit-fitting code; Dr. Stella Kafka for the CTIO 4.0m spectra, Nikhil van der Klaauw, Sean Samaroo, Emmett Goodman-Boyd, Jonathan Gagné and Dr. Inseok Song for useful discussions, and the staff of the Cerro Tololo Inter-American Observatory, particularly Edgardo Cosgrove, Arturo Gomez, Alberto Miranda, and Joselino Vasquez, for their help over the years.

REFERENCES

Adams, J. D., Stauffer, J. R., Monet, D. G., Skrutskie, M. F., & Beichman, C. A. 2001, AJ, 121, 2053

Allers, K. N. et al. 2007, ApJ, 657, 511

Baines, E. K. et al. 2012, ApJ, 761, 57

Baraffe, I., Chabrier, G., Allard, F., & Hauschildt, P. H. 1998, A&A, 337, 403

——. 2002, A&A, 382, 563

Barenfeld, S. A., Bubar, E. J., Mamajek, E. E., & Young, P. A. 2013, ApJ, 766, 6

Barrado y Navascues, D. 1998, A&A, 339, 831

Barrado y Navascués, D., Stauffer, J. R., Song, I., & Caillault, J. 1999, ApJ, 520, L123

Benedict, G. F. et al. 1999, AJ, 118, 1086

Bergfors, C. et al. 2010, A&A, 520, A54

Bessell, M. S. 1990, A&AS, 83, 357

——. 1991, AJ, 101, 662

Beuzit, J.-L. et al. 2004, A&A, 425, 997

Biller, B. A., & Close, L. M. 2007, ApJ, 669, L41

Caballero, J. A. 2009, A&A, 507, 251

Carson, J. et al. 2013, ApJ, 763, L32

Casagrande, L., Flynn, C., & Bessell, M. 2008, MNRAS, 389, 585

Castro, S., Porto de Mello, G. F., & da Silva, L. 1999, MNRAS, 305, 693

Chauvin, G., Lagrange, A.-M., Dumas, C., Zuckerman, B., Mouillet, D., Song, I., Beuzit, J.-L., & Lowrance, P. 2004, A&A, 425, L29

Cruz, K. L., Reid, I. N., Liebert, J., Kirkpatrick, J. D., & Lowrance, P. J. 2003, AJ, 126, 2421

Cutri, R. M. et al. 2003, 2MASS All Sky Catalog of point sources. (NASA/IPAC Infrared Science Archive.)

da Silva, L., Torres, C. A. O., de La Reza, R., Quast, G. R., Melo, C. H. F., & Sterzik, M. F. 2009, A&A, 508, 833

Daemgen, S., Siegler, N., Reid, I. N., & Close, L. M. 2007, ApJ, 654, 558

de la Reza, R., Torres, C. A. O., Quast, G., Castilho, B. V., & Vieira, G. L. 1989, ApJ, 343, L61

Delfosse, X., Forveille, T., Beuzit, J., Udry, S., Mayor, M., & Perrier, C. 1999, A&A, 344, 897

Delorme, P. et al. 2013, A&A, 553, L5

——. 2012, A&A, 548, A26

Desidera, S. et al. 2011, A&A, 529, A54

Donati, J.-F., Catala, C., Landstreet, J. D., & Petit, P. 2006, in Astronomical Society of the Pacific Conference Series, Vol. 358, Astronomical Society of the Pacific Conference Series, ed. R. Casini & B. W. Lites, 362

Dotter, A., Chaboyer, B., Jevremović, D., Kostov, V., Baron, E., & Ferguson, J. W. 2008, ApJS, 178, 89

Ducourant, C., Teixeira, R., Chauvin, G., Daigne, G., Le Campion, J.-F., Song, I., & Zuckerman, B. 2008, A&A, 477, L1

Eggen, O. J. 1991, AJ, 102, 2028

Faherty, J. K. et al. 2012, ApJ, 752, 56

Famaey, B., Siebert, A., & Jorissen, A. 2008, A&A, 483, 453

Fischer, D. A., & Marcy, G. W. 1992, ApJ, 396, 178

Franz, O. G. et al. 1998, AJ, 116, 1432

Gizis, J. E., & Bharat, R. 2004, ApJ, 608, L113

Gizis, J. E., Jao, W., Subasavage, J. P., & Henry, T. J. 2007, ApJ, 669, L45

Gizis, J. E., Reid, I. N., & Hawley, S. L. 2002, AJ, 123, 3356

Graham, J. A. 1982, PASP, 94, 244

Gregorio-Hetem, J., Lepine, J. R. D., Quast, G. R., Torres, C. A. O., & de La Reza, R. 1992, AJ, 103, 549

Hambly, N. C., Henry, T. J., Subasavage, J. P., Brown, M. A., & Jao, W. 2004, AJ, 128, 437

Henry, T. J., Ianna, P. A., Kirkpatrick, J. D., & Jahreiss, H. 1997, AJ, 114, 388

Henry, T. J., Jao, W., Subasavage, J. P., Beaulieu, T. D., Ianna, P. A., Costa, E., & Méndez, R. A. 2006, AJ, 132, 2360

Henry, T. J., Subasavage, J. P., Brown, M. A., Beaulieu, T. D., Jao, W., & Hambly, N. C. 2004, AJ, 128, 2460

Henry, T. J., Walkowicz, L. M., Barto, T. C., & Golimowski, D. A. 2002, AJ, 123, 2002

Hillenbrand, L. A., & White, R. J. 2004, ApJ, 604, 741

Hinkle, K. H., Wallace, L., & Livingston, W. 2003, in Bulletin of the American Astronomical Society, Vol. 35, American Astronomical Society Meeting Abstracts, 1260

Honeycutt, R. K. 1992, PASP, 104, 435

Jao, W., Henry, T. J., Subasavage, J. P., Brown, M. A., Ianna, P. A., Bartlett, J. L., Costa, E., & Méndez, R. A. 2005, AJ, 129, 1954

Jao, W., Henry, T. J., Subasavage, J. P., Winters, J. G., Riedel, A. R., & Ianna, P. A. 2011, AJ, 141, 117

Jao, W.-C., Henry, T. J., Beaulieu, T. D., & Subasavage, J. P. 2008, AJ, 136, 840

Jao, W.-C., Henry, T. J., Subasavage, J. P., Bean, J. L., Costa, E., Ianna, P. A., & Méndez, R. A. 2003, AJ, 125, 332

Johnson, D. R. H., & Soderblom, D. R. 1987, AJ, 93, 864

Kaufer, A., Stahl, O., Tubbesing, S., Nørregaard, P., Avila, G., Francois, P., Pasquini, L., & Pizzella, A. 1999, The Messenger, 95, 8

King, J. R., Villarreal, A. R., Soderblom, D. R., Gulliver, A. F., & Adelman, S. J. 2003, AJ, 125, 1980

Kiss, L. L. et al. 2011, MNRAS, 411, 117

Koen, C., Kilkenny, D., van Wyk, F., Cooper, D., & Marang, F. 2002, MNRAS, 334, 20

Landolt, A. U. 1992, AJ, 104, 340

——. 2007, AJ, 133, 2502

Lépine, S., & Simon, M. 2009, AJ, 137, 3632

López-Santiago, J., Micela, G., & Montes, D. 2009, A&A, 499, 129

Luhman, K. L., Stauffer, J. R., & Mamajek, E. E. 2005, ApJ, 628, L69

Lyo, A.-R., Lawson, W. A., & Bessell, M. S. 2004a, MNRAS, 355, 363

——. 2004b, MNRAS, 355, 363

Makarov, V. V., & Urban, S. 2000, MNRAS, 317, 289

Malo, L., Doyon, R., Lafrenière, D., Artigau, É., Gagné, J., Baron, F., & Riedel, A. 2013, ApJ, 762, 88

Mamajek, E. E. 2005, ApJ, 634, 1385

Mamajek, E. E. et al. 2013, ArXiv e-prints

Marois, C., Macintosh, B., Barman, T., Zuckerman, B., Song, I., Patience, J., Lafrenière, D., & Doyon, R. 2008, Science, 322, 1348

Mathieu, R. D., Baraffe, I., Simon, M., Stassun, K. G., & White, R. 2007, Protostars and Planets V, 411

McArthur, B. E., Benedict, G. F., Harrison, T. E., & van Altena, W. 2011, AJ, 141, 172

McCarthy, K., & White, R. J. 2012, AJ, 143, 134

Montes, D., López-Santiago, J., Fernández-Figueroa, M. J., & Gálvez, M. C. 2001, A&A, 379, 976

Nelan, E. P., Walborn, N. R., Wallace, D. J., Moffat, A. F. J., Makidon, R. B., Gies, D. R., & Panagia, N. 2004, AJ, 128, 323

Perryman, M. A. C. et al. 1997, A&A, 323, L49

Reid, I. N., & Hawley, S. L. 1999, AJ, 117, 343

Reid, I. N., Hawley, S. L., & Gizis, J. E. 1995, AJ, 110, 1838

Reiners, A., Basri, G., & Browning, M. 2009, ApJ, 692, 538

Riaz, B., Gizis, J. E., & Harvin, J. 2006, AJ, 132, 866

Rice, E. L., Faherty, J. K., & Cruz, K. L. 2010, ApJ, 715, L165

Riedel, A. R. 2012, PhD thesis, Georgia State University

Riedel, A. R., Murphy, S. J., Henry, T. J., Melis, C., Jao, W.-C., & Subasavage, J. P. 2011, AJ, 142, 104

Riedel, A. R. et al. 2010, AJ, 140, 897

Rodriguez, D. R., Bessell, M. S., Zuckerman, B., & Kastner, J. H. 2011, ApJ, 727, 62

Rojas-Ayala, B., Covey, K. R., Muirhead, P. S., & Lloyd, J. P. 2010, ApJ, 720, L113

Röser, S., Schilbach, E., Piskunov, A. E., Kharchenko, N. V., & Scholz, R.-D. 2011, A&A, 531, A92

Schlieder, J. E. 2011, PhD thesis, State University of New York at Stony Brook

Schlieder, J. E., Lépine, S., Rice, E., Simon, M., Fielding, D., & Tomasino, R. 2012a, AJ, 143, 114

Schlieder, J. E., Lépine, S., & Simon, M. 2010, AJ, 140, 119

——. 2012b, AJ, 143, 80

——. 2012c, AJ, 144, 109

Schmitt, J. H. M. M., Fleming, T. A., & Giampapa, M. S. 1995, ApJ, 450, 392

Scholz, R., Lo Curto, G., Méndez, R. A., Hambaryan, V., Costa, E., Henry, T. J., & Schwope, A. D. 2005, A&A, 439, 1127

Shkolnik, E., Liu, M. C., & Reid, I. N. 2009, ApJ, 699, 649

Shkolnik, E. L., Anglada-Escudé, G., Liu, M. C., Bowler, B. P., Weinberger, A. J., Boss, A. P., Reid, I. N., & Tamura, M. 2012, ApJ, 758, 56

Shkolnik, E. L., Hebb, L., Liu, M. C., Reid, I. N., & Collier Cameron, A. 2010, ApJ, 716, 1522

Shkolnik, E. L., Liu, M. C., Reid, I. N., Dupuy, T., & Weinberger, A. J. 2011, ApJ, 727, 6

Skrutskie, M. F. et al. 2006, AJ, 131, 1163

Soderblom, D. R., Nelan, E., Benedict, G. F., McArthur, B., Ramirez, I., Spiesman, W., & Jones, B. F. 2005, AJ, 129, 1616

Song, I., Zuckerman, B., & Bessell, M. S. 2003, ApJ, 599, 342

Torres, C. A. O., Quast, G. R., da Silva, L., de La Reza, R., Melo, C. H. F., & Sterzik, M. 2006, A&A, 460, 695

Torres, C. A. O., Quast, G. R., de La Reza, R., da Silva, L., Melo, C. H. F., & Sterzik, M. 2003, in Astrophysics and Space Science Library, Vol. 299, Open Issues in Local Star Formation, ed. J. Lépine & J. Gregorio-Hetem (Dordecht: Kluwer Academic Publishers), 83

Torres, C. A. O., Quast, G. R., Melo, C. H. F., & Sterzik, M. F. 2008, Handbook of Star Forming Regions, Volume II (San Francisco: ASP Press), 757

van Altena, W. F., Lee, J. T., & Hoffleit, E. D. 1995, The general catalogue of trigonometric [stellar] parallaxes, 4th ed., completely revised and enlarged (New Haven, CT: Yale University Observatory)

van Leeuwen, F., ed. 2007, Astrophysics and Space Science Library, Vol. 350, Hipparcos, the New Reduction of the Raw Data, ed. F. van Leeuwen (Berin: Springer)

Voges, W. et al. 1999, A&A, 349, 389

——. 2000, IAU Circ., 7432, 1

Webb, R. A., Zuckerman, B., Platais, I., Patience, J., White, R. J., Schwartz, M. J., & McCarthy, C. 1999, ApJ, 512, L63

Weinberger, A. J., Anglada-Escudé, G., & Boss, A. P. 2013, ApJ, 762, 118

Weis, E. W. 1993, AJ, 105, 1962

——. 1996, AJ, 112, 2300

Weis, E. W., Lee, J. T., Lee, A. H., Griese, III, J. W., Vincent, J. M., & Upgren, A. R. 1999, AJ, 117, 1037

West, A. A., & Basri, G. 2009, ApJ, 693, 1283

West, A. A., Hawley, S. L., Bochanski, J. J., Covey, K. R., Reid, I. N., Dhital, S., Hilton, E. J., & Masuda, M. 2008, AJ, 135, 785

White, R. J., & Basri, G. 2003, ApJ, 582, 1109

Winters, J. G., Henry, T. J., Jao, W., Subasavage, J. P., Finch, C. T., & Hambly, N. C. 2011, AJ, 141, 21

Yee, J. C., & Jensen, E. L. N. 2010, ApJ, 711, 303

Zacharias, N., Finch, C. T., Girard, T. M., Henden, A., Bartlett, J. L., Monet, D. G., & Zacharias, M. I. 2013, AJ, 145, 44

Zuckerman, B., Rhee, J. H., Song, I., & Bessell, M. S. 2011, ApJ, 732, 61

Zuckerman, B., & Song, I. 2004, ARA&A, 42, 685

Zuckerman, B., Song, I., & Bessell, M. S. 2004, ApJ, 613, L65

Zuckerman, B., Song, I., & Webb, R. A. 2001, ApJ, 559, 388

This 2-column preprint was prepared with the AAS LaTeX macros v5.2.

TABLE 1
YOUNG STAR STATISTICS

Association	All[a]			Within 25 pc[b]		
	Known members	M+ dwarfs	New members	Known members	M+ dwarfs	New members
ϵ Chameleontis	40	19	0	0	0	0
TW Hydra	41	31	2	0	0	0
β Pictoris	111	68	7	18	16	2
Octans	15	0	0	0	0	0
Tucana-Horologium	90	26	0	3	2	0
Columba	74	20	0	0	0	0
Carina	34	13	0	4	4	0
Argus	123	53	1	25	21	1
AB Doradus	182	74	1	35	24	1
Ursa Major	75	8	1	26	8	1
Unknown			2			1

NOTE.—The known members of nearby young associations, with new discoveries in this paper.

[a]Members are as defined in the following source papers: King et al. (2003),Zuckerman & Song (2004),Mamajek (2005),Torres et al. (2008),da Silva et al. (2009),Shkolnik et al. (2009),Lépine & Simon (2009),Rice et al. (2010),Schlieder et al. (2010),Shkolnik et al. (2011),Desidera et al. (2011),Kiss et al. (2011),Riedel et al. (2011),Rodriguez et al. (2011),Zuckerman et al. (2011),McCarthy & White (2012),Schlieder et al. (2012b),Schlieder et al. (2012c),Shkolnik et al. (2012). Quality of membership is as decided in the source paper and has not been re-evaluated here.

[b]25 pc is determined by trigonometric parallax if possible; otherwise, from published kinematic, photometric, or spectroscopic distances (in that order)

Table 2
Photometric Results

Name (1)	Alternate Name (2)	V_J (3)	R_{KC} (4)	I_{KC} (5)	No. of phot. Observations (6)	π filter (7)	σ (mag) (8)	No. of rel. Nights (9)	No. of Frames (10)	J (2MASS) (11)	H (2MASS) (12)	K_s (2MASS) (13)	spectral type[b] (14)	ref (15)	phot. dist. (pc) (16)	No. of Relations (17)	Notes (18)
NLTT 372	LP 404-32	15.87±0.04	14.66±0.03	13.12±0.05	3	V	0.014	21	97	11.64±0.02	11.00±0.03	10.72±0.02	M4.5V	1	47.39±7.47	12	a
G 131-26AB	NLTT 375	13.52±0.06	12.19±0.04	10.50±0.04	3	V	0.019	21	97	8.87±0.03	8.26±0.03	8.01±0.02	M4.0VeJ	2	10.74±1.67	12	a
SCR 0017-6645	RBS 38	12.45±0.02	11.37±0.01	10.00±0.01	2	V	0.035	11	54	8.56±0.02	7.93±0.04	7.70±0.02	M2.5Ve	2	14.82±2.69	12	
GJ 2006A	RBS 67	12.95±0.02	11.79±0.03	10.29±0.03	3	V	0.077	17	69	8.88±0.03	8.24±0.04	8.01±0.03	M3.5Ve	2	15.39±2.41	12	a
GJ 2006B		13.25±0.03	12.04±0.02	10.48±0.02	4	V	0.036	17	69	8.97±0.03	8.39±0.03	8.12±0.03	M3.5Ve	2	14.29±2.19	12	a
SCR 0103-5515ABC		15.48±0.03	14.00±0.02	12.07±0.02	2	R	0.021	11	49	10.16±0.02	9.58±0.03	9.24±0.02	M4.5Ve	2	12.86±1.97	12	
LP 467-16ABC		14.46±0.05	12.95±0.01	11.03±0.02	2	R	0.019	15	79	9.08±0.03	8.51±0.04	8.21±0.03	M4.5VeJ	2	7.88±1.22	12	
GJ 2022AC	G 269-153AB	13.56±0.04	12.26±0.01	10.62±0.05	3	R	0.067	14	31	9.20±0.04	8.66±0.05	8.24±0.03	M4.0VeJ	2	14.78±3.01	12	
GJ 2022B	G 269-153C	15.50±0.06	14.09±0.02	12.33±0.06	3	R	0.016	16	66	10.56±0.02	10.01±0.02	9.68±0.02	M4.5Ve	2	19.65±3.08	12	
LP 993-115		12.38±0.08	11.17±0.03	9.61±0.03	3	V	0.021	15	71	8.14±0.02	7.55±0.04	7.27±0.02	M3.5Ve	2	9.94±1.53	12	
LP 993-116AB	RBS 353	12.69±0.06	11.37±0.02	9.67±0.02	3	V	0.015	15	71	8.06±0.02	7.53±0.04	7.20±0.02	M4.0VeJ	2	7.62±1.21	12	
G 7-34		13.84±0.02	12.50±0.01	10.75±0.01	3	R	0.022	15	72	9.03±0.03	8.48±0.03	8.18±0.02	M4.0Ve	2	10.65±1.64	12	
G 39-29AB		12.56±0.05	11.31±0.01	9.70±0.02	3	V	0.015	13	70	8.17±0.02	7.62±0.02	7.33±0.02	M4.0VeJ	2	9.40±1.46	12	
LP 655-48		17.79±0.06	15.72±0.03	13.36±0.04	4	I	0.013	21	101	10.66±0.02	9.99±0.02	9.55±0.02	M6.5Ve	2	8.45±1.33	12	
LP 476-207ABC	HIP 23418	11.53±0.07	10.33±0.04	8.74±0.04	2	V	0.021	12	64	7.21±0.02	6.66±0.03	6.37±0.02	M3.0VeJ	2	6.28±0.97	12	
BD-21°1074BC		11.08±0.05	9.92±0.05	8.45±0.04	4	V	0.046	16	95	7.00±0.02	6.39±0.02	6.11±0.02	M3.0VeJ	2	6.37±1.00	12	a
BD-21°1074A	RBS 620	10.41±0.02	9.40±0.02	8.25±0.02	3	V	0.043	10	49	7.05±0.02	6.39±0.05	6.12±0.02	M1.5Ve	2	9.91±1.72	12	a
L 449-1AB	RBS 636	11.69±0.01	10.48±0.02	8.91±0.01	3	V	0.024	17	87	7.40±0.03	6.85±0.05	6.56±0.02	M3.5VeJ	2	7.01±1.08	12	a
SCR 0529-3239		13.79±0.02	12.50±0.01	10.80±0.01	2	R	0.014	11	49	9.22±0.03	8.61±0.04	8.32±0.03	M4.0Ve	2	12.83±1.98	12	
SCR 0613-2742AB		12.30±0.03	11.10±0.03	9.55±0.02	4	V	0.037	14	77	8.00±0.03	7.43±0.07	7.15±0.02	M4.0VeJ	2	8.98±1.41	12	
L 34-26		11.31±0.03	10.19±0.03	8.79±0.03	3	V	0.018	19	95	7.41±0.02	6.86±0.03	6.58±0.02	M3.0Ve	2	9.16±1.41	12	a
SCR 0757-7114		12.45±0.03	11.28±0.03	9.77±0.03	3	V	0.007	7	41	8.32±0.02	7.75±0.04	7.42±0.02	M3.5V	2	11.36±1.76	12	
SCR 1012-3124AB		13.51±0.02	12.20±0.01	10.51±0.03	2	V	0.015	11	59	8.85±0.02	8.26±0.05	7.99±0.03	M4.0VeJ	2	10.56±1.63	12	
TWA 8B		15.22±0.07	13.68±0.02	11.76±0.03	3	V	0.124	11	65	9.84±0.02	9.28±0.02	9.01±0.03	M5.0Ve	2	11.60±1.87	12	
TWA 8A	RBS 994	12.23±0.06	11.14±0.04	9.79±0.03	3	V	0.078	11	65	8.34±0.02	7.66±0.04	7.43±0.02	M4.0Ve	2	12.74±2.54	12	
SCR 1214-2345		13.96±0.02	12.57±0.02	10.78±0.03	2	V	0.010	11	54	9.07±0.02	8.56±0.05	8.23±0.03	M4.0Ve	2	10.66±1.75	12	
G 165-8AB	RBS 1280	12.02±0.09	10.77±0.05	9.15±0.07	3	R	0.018	31	181	7.56±0.02	7.00±0.02	6.72±0.02	M4.0VeJ	2	6.73±1.03	12	
SCR 1425-4113AB		12.54±0.15	11.48±0.17	10.06±0.11	2	V	0.078	11	57	8.55±0.03	7.91±0.03	7.61±0.02	M2.5VeJ	2	12.95±2.89	12	
GJ 1224	L 920-26	13.48±0.04	12.08±0.02	10.31±0.03	2	I	0.013	25	170	8.64±0.02	8.09±0.04	7.83±0.03	M4.0Ve	2	9.11±1.55	12	
G 141-29	LP 510-15	12.86±0.04	11.58±0.04	9.95±0.04	3	I	0.013	17	82	8.36±0.02	7.81±0.04	7.55±0.02	M4.0Ve	2	9.78±1.53	12	
SCR 1942-2045		14.33±0.05	12.98±0.02	11.25±0.01	2	R	0.019	9	48	9.60±0.02	9.03±0.02	8.76±0.02	M4.0Ve	2	14.62±2.31	12	
2MASS 2009-0113		14.47±0.05	12.98±0.03	11.16±0.03	3	I	0.015	14	71	9.40±0.03	8.83±0.03	8.51±0.02	M4.5Ve	2	10.81±1.79	12	
SCR 2010-2801AB		12.98±0.03	11.78±0.02	10.20±0.02	3	R	0.012	11	57	8.65±0.02	8.01±0.05	7.73±0.03	M4.0VeJ	2	11.18±1.83	12	
LEHPM2-0783	SIP 2019-5816	17.17±0.04	15.28±0.04	13.03±0.02	3	I	0.025	11	58	10.66±0.02	10.10±0.03	9.72±0.02	M6.5Ve	2	10.57±1.65	12	
L 755-19		12.47±0.02	11.31±0.01	9.81±0.02	2	R	0.018	11	56	8.39±0.03	7.76±0.03	7.50±0.03	M3.0Ve	2	12.01±1.88	12	
SCR 2033-2556		14.87±0.02	13.44±0.02	11.57±0.01	2	R	0.017	11	48	9.71±0.02	9.15±0.02	8.88±0.02	M4.5Ve	2	12.04±1.88	12	
SCR 2036-3607	RBS 1687	11.66±0.03	10.59±0.01	9.27±0.02	2	V	0.021	9	53	8.03±0.02	7.42±0.03	7.17±0.02	M2.5Ve	2	14.18±2.22	12	
GJ 799A	AT Mic A	10.36±0.03	9.08±0.03	7.40±0.03	3	V	0.064	18	131	5.81±0.03	5.20±0.05	4.94±0.04	M4.0VeJ	2	2.77±0.43	12	a
GJ 799B	AT Mic B	...	...	...		V	0.076	18	131	...	...	...	...	...	...	...	a c
LHS 3799	L 788-34	13.30±0.03	11.87±0.02	10.04±0.03	5	V	0.014	21	118	8.24±0.03	7.64±0.05	7.32±0.02	M4.5Ve	2	6.07±0.93	12	a
GJ 1284AB	RBS 2013	11.14±0.04	10.02±0.04	8.59±0.04	3	V	0.027	20	95	7.20±0.02	6.61±0.04	6.33±0.03	M3.0Ve	2	7.78±1.21	12	a
Previously Published																	
LHS 1302	G 159-3	14.49±0.05	13.00±0.02	11.16±0.03	5	R	0.021	26	141	9.41±0.02	8.84±0.02	8.55±0.02	M4.5Ve	2	11.04±1.88	12	
LHS 1358	G 159-46	13.58±0.03	12.31±0.03	10.66±0.02	2	R	0.015	11	58	9.06±0.03	8.52±0.03	8.17±0.02	M4.0V	1	12.54±1.94	12	
G 99-49		11.31±0.05	10.04±0.04	8.43±0.03	5	V	0.017	23	145	6.91±0.02	6.31±0.02	6.04±0.02	M3.5Ve	2	5.09±0.79	12	a
AP Col	LP 949-15	12.96±0.02	11.49±0.02	9.60±0.02	4	V	0.017	26	158	7.74±0.03	7.18±0.02	6.87±0.02	M4.5Ve	2	4.62±0.72	12	a
G 41-14ABC	LHS 6158	10.92±0.04	9.67±0.02	8.05±0.02	3	V	0.013	22	159	6.51±0.02	5.97±0.03	5.69±0.02	M3.5VeJ	2	4.39±0.69	12	a
TWA 27AB	2MA 1207-3932	19.95±0.20	17.99±0.07	15.92±0.05	5	I	0.015	12	54	13.00±0.03	12.39±0.03	11.95±0.03	M8 J	3	26.99±5.15	12	
LHS 2729	L 617-35	12.89±0.06	11.68±0.03	10.14±0.02	2	R	0.012	9	56	8.66±0.03	8.07±0.06	7.78±0.03	M3.5Ve	2	12.59±1.94	12	
LHS 2836	L 763-63	12.88±0.04	11.60±0.02	9.90±0.03	3	V	0.013	22	108	8.33±0.04	7.76±0.06	7.45±0.03	M4.0Ve	2	8.86±1.39	12	
GJ 1207	LHS 3255	12.25±0.04	10.99±0.05	9.43±0.05	5	V	0.199	27	124	7.97±0.02	7.44±0.08	7.12±0.02	M3.5Ve	2	9.36±1.59	12	a
LHS 4016AB	L 649-24	12.34±0.04	11.25±0.03	9.90±0.02	3	V	0.014	16	68	8.58±0.03	8.02±0.05	7.74±0.02	M2.5VeJ	2	17.18±2.65	12	

Note.—Photometry data collected on the sample.

[a] Astrometric results and relative photometry use new V filter data.

[b] References: (1) Reid et al. (1995); (2) This paper; (3) Gizis et al. (2007). "J" indicates joint spectral types from unresolved multiples.

[c] No independent photometry.

Table 3
Astrometric Results

Name (1)	R.A. Decl. (J2000)[a] (2) (3)	Filter (4)	N_{sea} (5)	[b]N_{frm} (6)	Coverage[b] (7)	Years (8)	[b]N_{ref} (9)	π(rel) (mas) (10)	π(corr) (mas) (11)	π(abs) (mas) (12)	μ (mas yr^{-1}) (13)	P.A. (deg) (14)	V_{tan} (km s^{-1}) (15)	Notes (16)
NLTT 372	00 08 51.79 +20 49 07.9	*V*	11s	97	1999.71–2011.89	12.18	7	10.50±1.44	1.16±0.07	11.66±1.44	147.8±0.3	121.1± 0.23	60.1	c
G 131-26AB	00 08 53.92 +20 50 25.4	*V*	11s	97	1999.71–2011.89	12.18	7	52.97±1.35	1.16±0.07	54.13±1.35	251.2±0.3	194.4± 0.11	22.0	c
SCR 0017-6645	00 17 23.53 −66 45 12.5	*V*	4s	54	2009.75–2012.88	3.13	9	24.71±1.73	0.90±0.10	25.61±1.73	93.6±1.8	101.1± 1.82	17.3	
GJ 2006A	00 27 50.24 −32 33 06.1	*V*	9s	69	2000.57–2010.82	10.25	7	29.49±2.50	0.65±0.11	30.14±2.50	115.0±0.6	109.6± 0.55	18.1	c
GJ 2006B	00 27 50.36 −32 33 23.9	*V*	9s	69	2000.57–2010.82	10.25	7	31.13±2.47	0.65±0.11	31.78±2.47	115.8±0.6	108.6± 0.53	17.3	c
SCR 0103-5515ABC	01 03 35.63 −55 15 56.2	*R*	6s	49	2007.82–2012.87	5.05	8	20.77±1.37	0.41±0.07	21.18±1.37	89.0±1.0	112.0± 1.24	19.9	
LP 467-16AB	01 11 25.41 +15 26 21.6	*R*	8s	79	1999.71–2009.57	9.86	7	44.88±1.77	0.91±0.16	45.79±1.78	222.9±0.6	122.7± 0.29	23.1	
GJ 2022AC	01 24 30.62 −33 55 01.6	...	...	...	...	...	...	...	...	...	...	...	...	d
GJ 2022B	01 24 30.62 −33 55 01.6	*R*	7s	66	1999.62–2011.53	11.91	7	38.40±2.13	0.40±0.07	38.80±2.13	206.0±0.7	127.5± 0.36	25.2	
LP 993-115	02 45 10.71 −43 44 32.4	*V*	8s	71	1999.62–2012.95	13.32	7	88.10±1.73	1.52±0.10	89.62±1.73	388.5±0.3	175.8± 0.06	20.5	
LP 993-116AB	02 45 14.32 −43 44 10.6	*V*	8s	71	1999.62–2012.95	13.32	7	82.60±2.08	1.52±0.10	84.12±2.08	367.6±0.4	175.3± 0.08	20.7	
G 7-34	04 17 18.52 +08 49 22.1	*R*	6s	72	1999.64–2007.83	8.19	9	71.98±1.26	1.29±0.19	73.27±1.27	395.2±0.7	161.2± 0.17	25.6	
G 39-29AB	04 38 12.59 +28 13 00.0	*V*	5s	70	2000.88–2005.06	4.18	8	76.01±2.00	2.60±0.40	78.61±2.04	403.2±1.8	103.0± 0.42	24.3	
LP 655-48	04 40 23.28 −05 30 08.1	*I*	10s	101	2003.95–2012.89	8.94	7	101.29±0.71	1.32±0.08	102.61±0.71	359.4±0.2	69.2± 0.06	16.6	
LP 476-207ABC	05 01 58.81 +09 58 58.8	*V*	5s	64	2000.06–2005.06	5.00	8	39.52±2.11	1.15±0.20	40.67±2.12	106.4±1.4	165.4± 1.31	12.4	
BD-21°1074BC	05 06 49.47 −21 35 03.8	*V*	7s	95	1999.81–2012.16	12.35	5	48.51±1.62	2.02±0.12	50.53±1.62	50.7±0.4	151.4± 0.84	4.8	c
BD-21°1074A	05 06 49.92 −21 35 09.2	*V*	4c	49	2000.06–2012.16	12.10	5	52.54±2.16	2.02±0.12	54.56±2.16	51.3±0.5	111.1± 1.06	4.5	c
L 449-1AB	05 17 22.91 −35 21 54.7	*V*	6c	87	2007.81–2012.96	5.15	6	83.60±1.34	0.78±0.12	84.38±1.35	280.5±0.8	234.5± 0.33	15.8	c
SCR 0529-3239	05 29 44.69 −32 39 14.2	*R*	3c	49	2008.85–2011.96	3.10	6	37.08±1.60	1.11±0.14	38.19±1.61	22.4±1.6	82.7± 6.37	2.8	
SCR 0613-2742AB	06 13 13.31 −27 42 05.5	*V*	4c	77	2009.93–2013.10	3.17	6	32.36±0.99	1.68±0.17	34.04±1.00	11.2±1.0	213.3±10.39	1.6	e
L 34-26	07 49 12.71 −76 42 06.6	*V*	8s	94	2006.21–2012.88	6.68	7	92.86±2.05	1.50±0.50	94.36±2.11	225.2±1.0	206.6± 0.46	11.1	c f
SCR 0757-7114	07 57 32.55 −71 14 53.8	*V*	3c	41	2009.92–2011.96	2.04	10	44.17±1.96	1.08±0.12	45.25±1.96	104.1±2.5	90.5± 1.94	10.9	
SCR 1012-3124AB	10 12 09.08 −31 24 45.2	*V*	3c	59	2010.01–2012.27	2.26	9	17.52±1.74	1.02±0.12	18.54±1.74	70.5±1.9	258.0± 2.61	18.0	
TWA 8B	11 32 41.17 −26 52 09.0	*V*	5s	65	2000.14–2011.16	11.02	6	19.90±1.44	1.32±0.12	21.22±1.44	75.3±0.3	253.9± 0.42	16.8	
TWA 8A	11 32 41.25 −26 51 55.9	*V*	5s	65	2000.14–2011.16	11.02	6	20.01±1.40	1.32±0.12	21.33±1.41	76.6±0.3	251.5± 0.41	17.0	
SCR 1214-2345	12 14 08.67 −23 45 17.0	*V*	4s	54	2010.16–2013.39	3.23	10	90.73±1.55	0.66±0.09	91.39±1.55	99.6±1.2	34.3± 1.32	5.2	
G 165-8AB	13 31 46.62 +29 16 36.6	*R*	10s	181	2000.14–2009.25	9.11	5	53.56±2.36	1.95±0.31	55.51±2.38	260.1±1.1	237.1± 0.46	22.2	
SCR 1425-4113AB	14 25 29.13 −41 13 32.4	*V*	3c	57	2010.16–2012.41	2.26	11	14.38±0.95	0.56±0.13	14.94±0.96	59.4±1.4	224.6± 2.62	18.8	
GJ 1224	18 07 32.85 −15 57 47.0	*I*	10s	170	2003.52–2012.52	9.00	7	125.04±0.92	1.50±0.50	126.54±1.05	702.3±0.4	241.0± 0.06	26.1	f
G 141-29	18 42 44.99 +13 54 17.1	*I*	7s	82	2003.52–2012.58	9.06	5	88.59±1.84	1.50±0.50	90.09±1.91	360.5±0.8	354.6± 0.18	18.3	f
SCR 1942-2045	19 42 12.82 −20 45 48.0	*R*	4c	48	2010.66–2013.38	2.72	10	62.37±1.07	1.00±0.18	63.37±1.09	144.7±1.4	183.7± 0.80	10.8	
2MASS 2009-0113	20 09 18.24 −01 13 38.2	*I*	8s	71	2004.73–2013.39	8.66	9	94.00±1.53	1.95±0.17	95.95±1.54	371.1±0.6	187.7± 0.16	18.3	
SCR 2010-2801AB	20 10 00.03 −28 01 41.2	*R*	4s	57	2008.71–2011.62	2.91	10	19.86±1.32	0.99±0.12	20.85±1.33	74.9±1.2	147.5± 1.73	17.0	
LEHPM2-0783	20 19 49.82 −58 16 43.0	*I*	4c	58	2006.37–2009.63	3.26	9	61.24±1.02	0.69±0.09	61.93±1.02	331.4±0.8	185.4± 0.22	25.4	
L 755-19	20 28 43.63 −11 28 30.8	*R*	6s	56	2007.82–2012.42	4.60	6	52.17±1.66	1.01±0.15	53.18±1.67	185.2±1.1	119.7± 0.69	16.5	
SCR 2033-2556	20 33 37.59 −25 56 52.1	*R*	5s	48	2008.71–2012.58	3.87	8	19.67±1.40	1.03±0.29	20.70±1.43	86.3±1.2	142.8± 1.59	19.8	
SCR 2036-3607	20 36 08.30 −36 07 11.5	*V*	4s	53	2009.62–2012.42	2.80	7	60.67±1.32	1.46±0.48	62.13±1.40	51.4±1.6	7.3± 2.81	3.9	
GJ 799A	20 41 51.14 −32 26 07.8	*V*	9s	131	2003.52–2012.58	9.06	7	98.10±1.58	2.72±0.14	100.82±1.59	449.9±0.6	149.4± 0.14	21.2	c
GJ 799B	20 41 51.14 −32 26 07.8	*V*	9s	131	2003.52–2012.58	9.06	7	100.06±1.63	2.72±0.14	102.78±1.64	433.4±0.6	137.2± 0.16	20.0	c
LHS 3799	22 23 07.00 −17 36 26.1	*V*	9s	118	2003.52–2012.70	9.18	6	137.70±1.86	0.47±0.14	138.17±1.87	769.1±0.4	157.7± 0.06	26.4	c
GJ 1284AB	23 30 13.45 −20 23 27.4	*V*	8s	95	2003.51–2011.51	8.00	5	66.35±2.27	1.55±0.29	67.90±2.29	363.5±0.9	121.1± 0.27	25.4	c
Previously Published Examples														
LHS 1302	01 51 04.09 −06 07 05.0	*R*	7c	141	1999.75–2005.96	6.25	6	100.14±1.89	0.64±0.06	100.78±1.89	597.1±0.9	115.5± 0.17	28.1	Henry et al. (2006)

TABLE 3—*Continued*

Name (1)	R.A. (J2000)[a] (2)	Decl. (J2000)[a] (3)	Filter (4)	N_{sea}[b] (5)	N_{frm} (6)	Coverage[b] (7)	Years[b] (8)	N_{ref} (9)	π(rel) (mas) (10)	π(corr) (mas) (11)	π(abs) (mas) (12)	μ (mas yr^{-1}) (13)	P.A. (deg) (14)	V_{tan} (km s^{-1}) (15)	Notes (16)
LHS 1358	02 12 54.63	+00 00 16.8	*R*	5s	58	1999.71–2003.86	4.15	5	64.09±2.07	1.18±0.13	65.27±2.07	558.3±1.3	086.1± 0.20	40.5	Riedel et al. (2010)
G 99-49	06 00 03.51	+02 42 23.6	*V*	7c	145	1999.91–2005.96	6.06	7	189.43±1.82	1.50±0.50	190.93±1.89	312.5±0.8	97.5± 0.24	7.8	Henry et al. (2006) [c] [f]
AP Col	06 04 52.16	−34 33 36.0	*V*	7c	158	2004.74–2011.23	6.48	14	118.26±0.97	0.95±0.11	119.21±0.98	342.0±0.5	4.6± 0.13	13.6	Riedel et al. (2011) [c]
G 41-14ABC	08 58 56.33	+08 28 26.0	*V*	7c	159	1999.97–2005.96	5.99	5	145.40±1.97	2.26±0.22	147.66±1.98	502.7±0.9	130.0± 0.20	16.1	Henry et al. (2006) [c]
TWA 27AB	12 07 33.46	−39 32 54.0	*I*	3c	54	2005.41–2007.56	2.14	7	17.93±1.03	0.58±0.05	18.51±1.03	66.7±1.5	250.0± 2.40	17.1	Gizis et al. (2007)
LHS 2729	13 23 38.02	−25 54 45.1	*R*	5s	56	2001.15–2005.09	3.94	12	70.32±1.52	1.16±0.14	71.48±1.53	633.9±1.3	249.8± 0.21	42.0	Riedel et al. (2010)
LHS 2836	13 59 10.45	−19 50 03.4	*V*	3c	108	2000.14–2004.18	4.04	8	91.22±0.86	1.64±0.23	92.86±0.89	573.4±1.0	252.0± 0.17	29.3	Riedel et al. (2010)
GJ 1207	16 57 05.73	−04 20 56.3	*V*	7c	124	1999.62–2005.71	6.09	10	113.36±1.44	2.03±0.44	115.39±1.51	608.5±0.8	127.1± 0.15	25.0	Henry et al. (2006) [c]
LHS 4016AB	23 48 36.06	−27 39 38.9	*V*	6s	68	2000.87–2009.75	8.87	6	40.75±1.54	0.50±0.19	41.25±1.55	595.3±0.4	246.2± 0.08	68.4	Riedel et al. (2010)

[a]coordinates are epoch and equinox 2000; each target's coordinates were extracted from 2MASS and then transformed to epoch 2000 using the proper motions and position angles listed here.

[b]'Coverage' and 'Years' run from the first to last data point; 'Seasons' counts observing semesters where a dataset was taken, and denotes if coverage was 'c'ontinuous (more than one night of data in all seasons) or 's'cattered.

[c]Astrometric results include new *V* filter data.

[d]Not using independent astrometry (see §5)

[e]The astrometric perturbation was incorporated into the final astrometric fit.

[f]Reference field was reddened, and a generic correction to absolute parallax was adopted.

TABLE 4

DATA USED TO CALCULATE UVWXYZ

Name	R.A. (J2000±mas)	Decl. (J2000±mas)	π (mas)	π Ref.	$\mu_{R.A.\cos Decl.}$ (mas yr^{-1})	$\mu_{Decl.}$ (mas yr^{-1})	μ Ref.	R.V. (km s^{-1})	R.V. Ref.
(1)	(2)	(3)	(4)	(5)	(6)	(7)	(8)	(9)	(10)
NLTT 372	00 08 51.788± 70	+20 49 07.86± 80	11.66±1.44	1	+120.7±12.1	−76.0±9.4	1	...	...
G 131-26AB	00 08 53.922± 70	+20 50 25.45± 80	54.13±1.35	1	−68.5±12.1	−243.0±9.4	2	...	...
SCR 0017-6645	00 17 23.524± 80	−66 45 12.46±110	25.61±1.73	1	+102.9± 1.0	−15.0±1.0	2	+11.4 ± 0.8	12
GJ 2006A	00 27 50.242± 70	−32 33 06.17± 70	30.97±1.76	1 1	+99.2± 1.3	−61.3±2.6	2	+8.4	13
GJ 2006B	00 27 50.362± 70	−32 33 23.91± 70	30.97±1.76	1 1	+117.2± 4.1	−31.5±5.8	2	...	...
SCR 0103-5515ABC	01 03 35.635± 60	−55 15 56.19± 80	21.18±1.37	1	+100.2± 2.0	−47.0±2.4	2	...	...
LP 467-16AB	01 11 25.412± 70	+15 26 21.62± 60	45.79±1.78	1	+181.8±12.1	−120.0±9.4	1	+4.0 ± 0.1	14
GJ 2022A	01 24 27.693± 60	−33 55 08.75± 60	39.50±1.28	1 3	+163.3±12.1	−125.0±9.5	1	+18.4 ± 1.0	3
GJ 2022C	01 24 27.692± 60	−33 55 08.75± 60	39.50±1.28	1 3	+154.8±12.1	−119.8±9.5	1	+19.4 ± 2.7	3
GJ 2022B	01 24 30.621± 60	−33 55 01.64± 60	39.50±1.28	1 3	+157.5±12.1	−125.1±9.4	1	+18.3 ± 0.5	3
LP 993-115	02 45 10.711± 70	−43 44 32.37± 60	87.37±1.33	1 1	+22.7±12.1	−387.2±9.4	1	...	...
LP 993-116AB	02 45 14.316± 70	−43 44 10.60± 60	87.37±1.33	1 1	+24.0±12.1	−366.1±9.4	1	...	...
G 7-34	04 17 18.521± 60	+08 49 22.06± 60	73.27±1.27	1	+121.6±12.1	−373.8±9.4	1	...	...
G 39-29AB	04 38 12.592±470	+28 13 00.00± 80	75.03±1.89	1 3	+386.9±12.2	−90.7±9.5	1	+35.7 ± 1.2	3
LP 655-48	04 40 23.282± 80	−05 30 08.12± 70	102.75±0.69	1 3	+330.2±12.1	+127.7±9.4	1	+29.9 ± 0.2	3
LP 476-207ABC	05 01 58.810± 60	+09 58 58.77± 60	40.18±2.07	1 5	+21.0±12.2	−102.6±9.5	1	+14.7 ± 3.7	15
BD-21°1074BC	05 06 49.472± 60	−21 35 03.83± 60	51.98±1.30	1 1	+33.1± 2.7	−33.2±2.0	2	+23.7 ± 1.7	15
BD-21°1074A	05 06 49.920± 60	−21 35 09.19± 60	51.98±1.30	1 1	+52.1± 1.7	−22.3±1.1	2	+21.2 ± 0.9	15
L 449-1AB	05 17 22.908± 60	−35 21 54.70± 60	84.38±1.35	1	−234.2±12.1	−162.6±9.5	1	...	...
SCR 0529-3239	05 29 44.686± 60	−32 39 14.17± 60	38.19±1.61	1	+12.5± 0.9	+13.4±1.8	2	...	...
SCR 0613-2742AB	06 13 13.308± 60	−27 42 05.46± 60	34.04±1.00	1	−13.1± 1.6	−0.3±1.3	2	+22.54± 1.16	1
L 34-26	07 49 12.709± 60	−76 42 06.60± 60	94.36±2.11	1	−102.4± 1.1	−191.9±1.1	2	+0.9	16
SCR 0757-7114	07 57 32.554± 60	−71 14 53.81± 70	45.25±1.96	1	+86.7± 1.3	+20.6±1.3	2	...	...
SCR 1012-3124AB	10 12 09.085± 60	−31 24 45.20± 60	18.54±1.74	1	−74.8± 1.1	−9.4±1.0	2	+14.69± 0.53	13
TWA 8B	11 32 41.165± 70	−26 52 09.04± 70	21.28±1.01	1 1	−95.3± 2.2	−28.6±4.7	2	+8.93± 0.27	17
TWA 8A	11 32 41.247± 70	−26 51 55.94± 70	21.28±1.01	1 1	−95.3± 2.2	−28.6±4.7	2	+8.34± 0.48	17
SCR 1214-2345	12 14 08.666± 80	−23 45 17.06± 70	91.39±1.55	1	+42.4± 1.1	+85.0±3.4	2	...	...
G 165-8AB	13 31 46.620± 70	+29 16 36.54± 60	55.51±2.38	1	−244.1± 4.2	−132.4±4.8	2	−7.5 ± 6.5	15
SCR 1425-4113AB	14 25 29.128± 60	−41 13 32.40± 60	14.94±0.96	1	−46.8± 2.1	−49.2±1.7	2	−1.2 ± 1.3	1
GJ 1224	18 07 32.853± 60	−15 57 47.05± 60	126.99±1.01	1 4	−620.3±12.1	−339.9±9.4	1	−34.8 ± 1.7	15
G 141-29	18 42 44.985± 60	+13 54 17.05± 70	90.18±1.88	1 4	−39.9±12.1	+359.2±9.5	1	−33.2	15
SCR 1942-2045	19 42 12.818± 60	−20 45 47.97± 60	62.75±0.90	1 3	−17.2± 2.5	−147.9±2.6	2	−1.7 ± 0.2	3
2MASS 2009-0113	20 09 18.242± 60	−01 13 38.19± 60	95.95±1.54	1	−55.7±12.1	−367.5±9.4	1	...	...
SCR 2010-2801AB	20 10 00.035± 60	−28 01 41.18± 60	20.85±1.33	1	+40.7± 3.0	−62.0±1.7	2	...	...
LEHPM2-0783	20 19 49.818± 60	−58 16 43.02± 60	61.93±1.02	1	−37.2±12.1	−329.7±9.5	1	...	...
L 755-19	20 28 43.624± 60	−11 28 30.82± 60	53.18±1.67	1	+155.0±12.1	−91.4±9.5	1	...	...
SCR 2033-2556	20 33 37.593± 60	−25 56 52.15± 60	20.70±1.43	1	+52.8± 1.7	−75.9±1.3	2	...	...
SCR 2036-3607	20 36 08.299± 60	−36 07 11.48± 60	62.13±1.40	1	+5.4± 1.7	+43.3±0.9	2	+2	16
GJ 799A	20 41 51.152±130	−32 26 08.00±190	101.31±0.75	1 1 3 3 4 4	+223.2±12.1	−386.9±9.4	1	−3.7 ± 3.0	14
GJ 799B	20 41 51.161±130	−32 26 09.98±190	101.31±0.75	1 1 3 3 4 4	+288.8±12.1	−317.5±9.4	1	−2.7 ± 3.0	14
LHS 3799	22 23 06.997± 60	−17 36 26.12± 70	137.69±1.75	1 4	+285.9±12.1	−711.3±9.4	1	−2.1 ± 1.1	15
GJ 1284AB	23 30 13.447± 60	−20 23 27.44± 60	65.79±1.86	1 5	+305.3±12.1	−187.5±9.5	1	−5.7	16
LHS 1302	01 51 04.094± 80	−06 07 05.07± 80	100.78±1.89	6	+531.8±12.1	−257.9±9.4	6	...	...
LHS 1358	02 12 54.630± 60	+00 00 16.81± 70	65.27±2.07	7	+551.2±12.1	+37.8±9.5	7	...	...
G 99-49	06 00 03.515± 60	+02 42 23.63± 60	190.77±1.86	4 6	+305.2±12.1	−41.7±9.5	6	+28.7 ± 0.7	15
AP Col	06 04 52.157± 60	−34 33 35.98± 60	119.21±0.98	8	+21.4±12.1	+341.2±9.4	8	+22.4 ± 0.3	8
G 41-14ABC	08 58 56.332± 60	+08 28 26.00±100	147.66±1.98	6	+371.2± 3.5	−323.4±2.8	2	−6.4 ±19.0	15
TWA 27AB	12 07 33.463± 60	−39 32 54.01± 60	18.95±0.37	9 10 11	−68.5±12.2	−22.5±9.5	9	+7.5 ± 2.0	18
LHS 2729	13 23 38.020± 60	−25 54 45.12± 70	71.48±1.53	7	−600.9±12.1	−218.3±9.5	7	...	...
LHS 2836	13 59 10.422± 90	−19 50 03.62± 60	92.86±0.89	7	−551.2±12.1	−177.0±9.5	7	−15.8	15
GJ 1207	16 57 05.729± 60	−04 20 56.29± 60	115.26±1.50	4 6	+479.1±12.1	−367.1±9.5	6	−4.2 ± 1.6	15
LHS 4016AB	23 48 36.062± 60	−27 39 38.87± 70	41.25±1.55	7	−551.9±12.1	−239.8±9.5	7	+25.3 ± 0.55	19

NOTE.—References in this table: 1: This paper, 2: UCAC4 (Zacharias et al. 2013), 3: Shkolnik et al. (2012), 4: YPC (van Altena et al. 1995), 5: HIPPARCOS (van Leeuwen 2007), 6: Henry et al. (2006), 7: Riedel et al. (2010), 8: Riedel et al. (2011), 9: Gizis et al. (2007) 10: Biller & Close (2007), 11: Ducourant et al. (2008), 12: Malo et al. (2013), 13: Malo et al. *in preparation*, 14: Montes et al. (2001), 15: Gizis et al. (2002), 16: Torres et al. (2006), 17: Shkolnik et al. (2011), 18: Rice et al. (2010), 19: Shkolnik et al. (2010). Parallaxes

of multiple components in the same system have been combined, and are represented by duplicate references in the parallax column. All positions and position errors are taken from 2MASS (Skrutskie et al. 2006), and adjusted to epoch 2000.0 equinox J2000 using the proper motions listed here.

TABLE 5

DEBLENDED MAGNITUDES FOR ISOCHRONES

Name (1)	V (2)	I (3)	J (4)	K (5)	M_V (6)	$V-K$ (7)	Deblend[a] (8)
NLTT 372	15.87	13.12	11.64	10.72	11.20	5.15	
G 131-26A	13.94	10.98	9.40	8.81	12.61	5.13	K
G 131-26B	14.76	11.61	9.90	9.27	13.43	5.49	K
SCR 0017-6645	12.45	10.00	8.56	7.70	9.49	4.75	
GJ 2006A	12.95	10.29	8.88	8.01	10.40	4.94	
GJ 2006B	13.25	10.48	8.97	8.12	10.70	5.13	
SCR 0103-5515A	16.07	12.70	10.83	9.91	12.70	6.16	K
SCR 0103-5515B	16.43	12.97	11.04	10.11	13.06	6.32	K
SCR 0103-5515C	23.39	18.14	14.92	13.69	20.02	9.70	K
LP 467-16A	14.76	11.41	9.53	8.67	13.06	6.09	K
LP 467-16B	15.99	12.36	10.27	9.36	14.29	6.63	K
GJ 2022A	14.27	11.34	9.93	8.97	12.25	5.30	V
GJ 2022C	14.35	11.40	9.98	9.02	12.33	5.33	V
GJ 2022B	15.50	12.33	10.56	9.68	13.48	5.82	
LP 993-115	12.38	9.61	8.14	7.27	12.09	5.11	
LP 993-116A	13.02	9.58	8.49	7.63	12.73	5.39	i'
LP 993-116B	14.14	10.54	9.27	8.40	13.85	5.74	i'
G 7-34	13.84	10.75	9.03	8.18	13.16	5.66	
G 39-29A	13.03	10.23	8.75	7.91	12.41	5.12	K
G 39-29B	13.69	10.74	9.14	8.28	13.07	5.41	K
LP 655-48	17.79	13.36	10.66	9.55	17.85	8.24	
LP 476-207A	12.46	9.75	8.30	7.48	10.48	4.98	SB,K
LP 476-207B	13.56	10.41	8.65	7.76	11.58	5.80	K
LP 476-207C	12.46	9.75	8.30	7.48	10.48	4.98	SB,K
BD-21°1074B	11.44	8.86	7.47	6.60	10.02	4.84	R
BD-21°1074C	12.44	9.71	8.14	7.21	11.02	5.23	R
BD-21°1074A	10.41	8.25	7.05	6.12	8.99	4.29	
L 449-1A	12.05	9.32	7.87	7.05	11.68	5.00	R
L 449-1B	13.06	10.17	8.54	7.66	12.69	5.40	R
SCR 0529-3239	13.79	10.80	9.22	8.32	11.70	5.47	
SCR 0613-2742A	12.78	10.07	8.57	7.72	10.44	5.06	R
SCR 0613-2742B	13.41	10.60	8.98	8.11	11.07	5.30	R
L 34-26	11.31	8.79	7.41	6.58	11.18	4.73	
SCR 0757-7114	12.45	9.77	8.32	7.42	10.73	5.03	
SCR 1012-3124A	14.25	11.25	9.59	8.74	10.59	5.51	V
SCR 1012-3124B	14.28	11.27	9.61	8.75	10.62	5.53	V
TWA 8B	15.22	11.76	9.84	9.01	11.86	6.21	
TWA 8A	12.23	9.79	8.34	7.43	8.87	4.80	
SCR 1214-2345	13.96	10.78	9.07	8.23	13.80	5.73	
G 165-8A	12.64	9.80	8.23	7.40	11.36	5.24	K
G 165-8B	12.93	10.02	8.40	7.56	11.65	5.37	K
SCR 1425-4113A	13.29	10.81	9.30	8.37	9.16	4.92	SB
SCR 1425-4113B	13.29	10.81	9.30	8.37	9.16	4.92	SB
GJ 1224	13.48	10.31	8.64	7.83	14.00	5.65	
G 141-29	12.86	9.95	8.36	7.55	12.64	5.31	
SCR 1942-2045	14.33	11.25	9.60	8.76	13.31	5.57	
2MASS 2009-0113	14.47	11.16	9.40	8.51	14.38	5.96	
SCR 2010-2801A	13.62	10.85	9.32	8.41	10.22	5.21	R
SCR 2010-2801B	13.86	11.06	9.49	8.56	10.46	5.30	R
LEHPM2-0783	17.17	13.03	10.66	9.72	16.13	7.46	
L 755-19	12.47	9.81	8.39	7.50	11.10	4.97	
SCR 2033-2556	14.87	11.57	9.71	8.88	11.45	5.99	
SCR 2036-3607	11.66	9.27	8.03	7.17	10.63	4.49	
GJ 799A	11.09	8.14	6.55	5.69	11.12	5.40	V
GJ 799B	11.13	8.17	6.57	5.71	11.16	5.42	V
LHS 3799	13.30	10.04	8.24	7.32	13.99	5.98	
GJ 1284A	11.89	9.34	7.95	7.08	10.98	4.81	SB
GJ 1284B	11.89	9.34	7.95	7.08	10.98	4.81	SB

TABLE 5—*Continued*

Name (1)	V (2)	I (3)	J (4)	K (5)	M_V (6)	$V-K$ (7)	Deblend[a] (8)
LHS 1302	14.49	11.16	9.41	8.55	14.51	5.94	
LHS 1358	13.58	10.66	9.06	8.17	12.65	5.41	
G 99-49	11.31	8.43	6.91	6.04	12.71	5.27	
AP Col	12.96	9.60	7.74	6.87	13.34	6.09	
G 41-14A	12.07	9.27	7.78	6.97	12.92	5.10	K,SB
G 41-14B	12.07	9.27	7.78	6.97	12.92	5.10	K,SB
G 41-14C	12.21	9.20	7.56	6.72	13.06	5.49	K
TWA 27A	19.95	15.92	13.00	11.96	16.34	7.99	K
TWA 27B	28.91	22.74	18.33	16.94	25.30	11.97	K
LHS 2729	12.89	10.14	8.66	7.78	12.16	5.11	
LHS 2836	12.88	9.90	8.33	7.45	12.72	5.44	
GJ 1207	12.25	9.43	7.97	7.12	12.56	5.13	
LHS 4016A	13.09	10.65	9.34	8.50	11.17	4.59	SB
LHS 4016B	13.09	10.65	9.34	8.50	11.17	4.59	SB

[a]Band of known Δ mag used to deblend the photometry, or SB if system was identified only as a spectroscopic binary. No entry is given for single stars because deblending is not required.

TABLE 6

PHOTOMETRIC AND SPECTROSCOPIC PROPERTIES

Name	M_V	$V-K_S$	$\log \frac{L_X}{L_{bol}}$	$\log L_X$	Variability		H-α	Na I	K I
	(mag)	(mag)		(erg $^{-1}$)	filter	(mag)	EW Å	Index	EW Å
(1)	(2)	(3)	(4)	(5)	(6)	(7)	(8)	(9)	(10)
NLTT 372	11.20	5.15	(−2.22)	(29.73)	V	0.014			
G 131-26AB	12.19	5.51	−3.28	28.40	V	0.019	-3.5	1.25	2.2
SCR 0017-6645	9.49	4.75	−3.01	29.49	V	0.035	-4.8	1.11	0.5
GJ 2006A	10.40	4.94	−2.96	29.50	V	0.077	-5.6	1.13	0.6
GJ 2006B	10.70	5.13			V	0.036	-10.0	1.15	1.1
SCR 0103-5515ABC	12.11	6.24	(−4.57)	(27.40)	R	0.021	-14.5	1.25	3.0
LP 467-16AB	12.76	6.25	−3.08	28.62	R	0.019	-9.9	1.19	2.5
GJ 2022AC	11.54	5.32	−2.70	29.08	R	0.067	-9.4	1.23	2.1
GJ 2022B	13.48	5.82	(−4.52)	(26.87)	R	0.016	-6.3	1.24	2.4
LP 993-115A	12.09	5.11	(−5.43)	(26.14)	V	0.021	-1.6	1.19	1.5
LP 993-115BC	12.40	5.49	−3.24	28.35	V	0.015	-7.7	1.25	2.2
G 7-34	13.16	5.66	−3.09	28.24	R	0.022	-8.4	1.19	2.0
G 39-29AB	11.94	5.23	−3.00	28.68	V	0.015	-4.7	1.19	2.1
LP 655-48	17.85	8.24	−2.74	27.63	I	0.013	-17.8	1.35	5.0
LP 476-207ABC	9.55	5.16	−3.11	29.50	V	0.021	-8.9	1.14	1.1
BD-21°1074BC	9.66	4.97	−3.24	29.58	V	0.046	-5.2	1.13	0.8
BD-21°1074A	8.99	4.29			V	0.043	-2.0	1.10	0.7
L 449-1AB	11.32	5.13	−3.02	28.88	V	0.024	-5.9	1.21	1.6
SCR 0529-3239	11.70	5.47	−3.09	28.77	R	0.014	-6.1	1.18	1.5
SCR 0613-2742AB	9.96	5.16	−2.95	29.50	V	0.037	-6.0	1.10	0.8
L 34-26	11.18	4.73	−3.07	28.76	V	0.018	-4.9	1.18	1.0
SCR 0757-7114	10.73	5.03	(−5.55)	(26.54)	V	0.007	0.3	1.17	0.7
SCR 1012-3124AB	9.85	5.52	(−4.84)	(27.76)	V	0.015	-5.7	1.08	0.6
TWA 8B	11.86	6.21	−2.99	29.86	V	0.124	-13.8	1.14	1.5
TWA 8A	8.87	4.80			V	0.078	-9.2	1.12	0.5
SCR 1214-2345	13.76	5.73	−3.00	28.12	V	0.010	-7.4	1.35	3.6
G 165-8AB	10.74	5.30	−3.16	29.02	R	0.018	-7.3	1.17	1.3
SCR 1425-4113AB	8.41	4.92	(−5.02)	(27.97)	V	0.078	-7.0	1.08	0.6
GJ 1224	14.00	5.65	−3.03	27.97	I	0.013	-4.3	1.26	3.1
G 141-29	12.64	5.31	−3.27	28.16	I	0.013	-4.7	1.22	2.0
SCR 1942-2045	13.32	5.57	−2.89	28.37	R	0.019	-5.4	1.24	2.5
2MASS 2009-0113	14.38	5.96	−3.31	27.64	I	0.015	-5.5	1.28	3.3
SCR 2010-2801AB	9.58	5.25	−3.03	29.60	R	0.012	-9.8	1.15	1.1
LEHPM2-0783	16.13	7.46	−2.20	28.57	I	0.025	-26.6	1.34	5.6
L 755-19	11.10	4.97	−3.25	28.69	R	0.018	-5.0	1.17	1.1
SCR 2033-2556	11.45	5.99	−3.10	29.03	R	0.017	-12.6	1.18	2.0
SCR 2036-3607	10.63	4.49	−2.94	29.02	V	0.021	-3.2	1.13	0.9
GJ 799AB	10.39	4.67	−2.85	29.52	V	0.064	-10.8	1.16	1.5
LHS 3799	13.99	5.98	−3.20	27.90	V	0.014	-3.8	1.31	2.9
GJ 1284AB	10.23	4.81	−3.23	29.00	V	0.027	-3.7	1.17	1.0
LHS 1302	14.51	5.94	−3.32	27.58	R	0.021	-3.6	1.27	3.1
LHS 1358	12.85	5.41	−3.23	28.22	R	0.015			
G 99-49	12.71	5.27	−3.40	27.98	V	0.017	-4.6	1.22	2.1
AP Col	13.34	6.09	−2.92	28.49	V	0.017	-18.4	1.17	2.2
G 41-14ABC	11.77	5.23	−2.94	28.81	V	0.013	-4.0	1.22	2.0
TWA 27A	16.34	8.00	(−3.30)	(27.58)	I	0.015			
LHS 2729	12.16	5.11	−3.21	28.33	R	0.012	-3.4	1.16	1.7
LHS 2836	12.72	5.44	−3.22	28.25	V	0.013	-3.7	1.22	2.0
GJ 1207	12.56	5.13	−3.11	28.30	V	0.199	-4.9	1.17	1.3
LHS 4016AB	10.42	4.60	−3.14	28.94	V	0.014	-2.1	1.14	1.0

NOTE.—Errors on X-ray values are less than 25%. Errors on spectroscopic EW measures are roughly 0.2Å. Errors on the Na I index are 0.05. Values in parentheses are upper limits. Three systems have multiple resolved components within the RASS positional uncertainties, and have combined X-ray luminosities

TABLE 7
YOUNG STAR RESULTS

Name	Kinematic			BANYAN		Isochrone	Gravity	Hα age	Association	Other
	Match	γ	R.V.	Match	Prob (%)	Range	Match	(Gyr)		References
(1)	(2)	(3)	(4)	(5)	(6)	(7)	(8)	(9)	(10)	(11)
NLTT 372				Field	99.9	ABD–βPic	N/A	N/A		
G 131-26AB				Field	99.9	Field–ABD	Old	<4.5		
SCR 0017-6645	β Pic	0.24	+11.0	β Pic	99.9	βPic	Young	<1.6	β Pictoris	Riedel (2012), Malo et al. (2013)
GJ 2006AB	β Pic	1.86	+11.4[a]	β Pic	99.9	βPic	Young	<3.0	β Pictoris	Riedel (2012)
SCR 0103-5515ABC	Carina	1.68	+14.3[a]	Tuc-Hor	98.9	TWA–βPic	Young	<6.0	Unknown	(Delorme et al. 2012 Tucana-Horologium)
LP 467-16AB	β Pic	0.46	+4.0	β Pic	99.0	βPic–Field	Young	<6.0	β Pictoris	Riedel (2012), Malo et al. (2013)
GJ 2022ABC	AB Dor	0.09	+18.4	AB Dor	99.9	Field	Young	<4.5	AB Doradus	Riedel (2012), Shkolnik et al. (2012)
LP 993-115ABC				Field	99.9	Field	Old	<3.0		
G 7-34	AB Dor	2.82	+18.0[a]	AB Dor	99.9	Field	Young	<4.5	AB Doradus	Riedel (2012)
G 39-29AB				Field	99.9	Field	Old	<4.5		
LP 655-48				Field	99.9	Field	Old	<7.5		
LP 476-207ABC	β Pic	0.64	+14.7	β Pic	99.9	βPic	Young	<2.0	β Pictoris	Song et al. (2003)
BD-21°1074ABC	β Pic	0.72	+21.2	β Pic	99.9	βPic	Young	<1.0	β Pictoris	Torres et al. (2008)
L 449-1AB	Ursa Major	1.69	−2.3[a]	Field	99.9	Field	Old	<3.0	Ursa Major?	Riedel (2012)
SCR 0529-3239	β Pic	2.74	+24.8[a]	β Pic	99.9	βPic–Field	Young	<4.5	β Pictoris	Riedel (2012)
SCR 0613-2742AB	β Pic	0.44	+22.5	β Pic	99.9	βPic	Young	<4.5	β Pictoris	Riedel (2012), Malo et al. (2013)
L 34-26	Ursa Major	3.87	+6.7[a]	Field	99.9	Field	Old	<2.0		
SCR 0757-7114				Field	99.9	βPic–ABD	Young?	>3.0		
SCR 1012-3124AB	TW Hya	3.20	+14.7	TW Hya	99.9	TWA–βPic	Young	<4.5	TW Hydra	Riedel (2012)
TWA 8AB	TW Hya	3.26	+8.3	TW Hya	99.9	TWA	Young	<4.5	TW Hydra	Webb et al. (1999)
SCR 1214-2345				Field	99.9	Field	Old	<4.5		
G 165-8AB	Carina	0.06	−7.5	Columba	74.7	βPic–Field	Young	<4.0	Unknown	Riedel (2012)
SCR 1425-4113AB	β Pic	0.59	−3.7	TW Hya	75.0	>TWA	Young	<1.6	TW Hydra?	Riedel (2012)
GJ 1224				Field	99.9	Field	Old	<4.5		
G 141-29	Hyades	3.68	−38.2[a]	Field	99.9	Field	Old	<4.5		
SCR 1942-2045				Field	99.9	Field	Old	<4.5		
2MASS 2009-0113				Field	99.9	Field	Old	<6.0		
SCR 2010-2801AB	β Pic	2.05	−10.0[a]	β Pic	99.9	TWA–βPic	Young	<4.5	β Pictoris	Riedel (2012), Malo et al. (2013)
LEHPM2-0783				Field	99.9	TWA–Field	Old	<7.5		
L 755-19	Argus	3.21	−25.4	Argus	99.9	βPic–Field	Old	<2.0	Argus?	Riedel (2012)
SCR 2033-2556	β Pic	0.75	−9.1[a]	β Pic	99.9	TWA	Young	<6.0	β Pictoris	Riedel (2012), Malo et al. (2013)
SCR 2036-3607	Ursa Major	1.22	+20.9[a]	Field	99.9	Field	Young	<1.6		
GJ 799AB	β Pic	0.93	−3.7	β Pic	99.9	βPic	Young	<4.5	β Pictoris	Barrado y Navascués et al. (1999)
LHS 3799				Field	94.1	Field	Old	<4.5		
GJ 1284AB	Columba	0.27	−3.7[a]	β Pic	51.9	βPic–Field	Old	<2.0		
LHS 1302	Columba	2.89	+10.2[a]	Field	87.6	Field	Old	<6.0		
LHS 1358	Hyades	1.13	+22.9[a]	Field	99.9	Field	N/A	N/A		
G 99-49				Field	99.9	Field	Old	<3.0		(Montes et al. 2001 Hyades)
AP Col	Argus	0.18	+22.4	Argus	99.9	βPic–Field	Young	<6.0	Argus	Riedel et al. (2011)
G 41-14ABC	Ursa Major	0.51	−6.4	Field	99.9	Field	Old	<3.0		
TWA 27AB	TW Hya	0.23	+7.5	TW Hya	99.9	TW Hya	N/A	N/A	TW Hydra	Gizis et al. (2002)
LHS 2729				Field	99.9	Field	Old	<3.0		
LHS 2836				Field	99.9	Field	Old	<4.5		

TABLE 7—*Continued*

Name	Kinematic			BANYAN		Isochrone	Gravity	Hα age	Association	Other
	Match	γ	R.V.	Match	Prob (%)	Range	Match	(Gyr)		References
(1)	(2)	(3)	(4)	(5)	(6)	(7)	(8)	(9)	(10)	(11)
GJ 1207				Field	99.9	Field	Old	<3.0		
LHS 4016AB				Field	99.9	Field	Old	<1.6		

[a]R.V. is actually a best-fit R.V. from the kinematic fitting.

Table 8
Nearby Young Associations

Name	U (km s^{-1})	σ_U (km s^{-1})	V (km s^{-1})	σ_V (km s^{-1})	W (km s^{-1})	σ_W (km s^{-1})	min X (pc)	max X (pc)	min Y (pc)	max Y (pc)	min Z (pc)	max Z (pc)	Age (Myr)
(1)	(2)	(3)	(4)	(5)	(6)	(7)	(8)	(9)	(10)	(11)	(12)	(13)	(14)
ϵ Cha	-11.0	1.2	-19.9	1.2	-10.4	1.6	+34	+60	-105	-78	-44	-12	6[a]
TW Hya	-10.5	0.9	-18.0	1.5	-4.9	0.9	+2	+34	-61	-26	+10	+27	8[a]
β Pic	-10.1	2.1	-15.9	0.8	-9.2	1.0	-32	+76	-33	21	-29	-1	12[a]
Octans	-14.5	0.9	-3.6	1.6	-11.2	1.4	-79	+142	-138	-60	-85	-38	20
Tuc-Hor	-9.9	1.5	-20.9	0.8	-1.4	0.9	-61	+43	-47	-4	-44	-30	30
Columba	-13.2	1.3	-21.8	0.8	-5.9	1.2	-106	+9	-168	+1	-99	+6	30
Carina	-10.2	0.4	-23.0	0.8	-4.4	1.5	-2	+33	-154	-39	-33	+5	30
Argus	-22.0	0.3	-14.4	1.3	-5.0	1.3	-55	+64	-154	-6	-67	+8	50
AB Dor	-6.8	1.3	-27.2	1.2	-13.3	1.6	-94	+73	-131	+58	-66	+23	125[b]
Pleiades[c]	-6.6	0.4	-27.6	0.3	-14.5	0.3	-134	-108	+14	+40	-66	-40	125[b]
Castor[d]	-10.7	3.5	-8.0	2.4	-9.7	3.0	...	...	...	...	...	...	200
UMa[e]	+14.56	2.28	+2.81	1.75	-8.37	3.42	...	...	...	...	...	...	500
Hyades[f]	-41.1	2.0	-19.2	2.0	-1.4	2.0	-53	-33	-9.3	+10.7	-27.3	+7.3	650

Note.—All data (unless otherwise specified) from Torres et al. (2008).

[a]Only these ages are known with any degree of certainty or corroboration.

[b]Age from Luhman et al. (2005)

[c]Dimensions Soderblom et al. (2005), 13 pc tidal radius Adams et al. (2001)

[d]Barrado y Navascues (1998)

[e]King et al. (2003)

[f]Röser et al. (2011)

TABLE 9
UVWXYZ KINEMATICS

Name	U (km s^{-1})	V (km s^{-1})	W (km s^{-1})	X (pc)	Y (pc)	Z (pc)
(1)	(2)	(3)	(4)	(5)	(6)	(7)
NLTT 372	...	...	...	−21.86±2.73	+61.00±7.61	−56.25±7.01
G 131-26AB	...	...	...	−4.71±0.12	+13.13±0.33	−12.10±0.30
SCR 0017-6645	−11.30± 1.12	−16.71± 0.87	−9.19± 0.63	+15.49±1.05	−19.72±1.33	−29.92±2.02
GJ 2006A	...	...	...	+4.04±0.23	−1.10±0.06	−32.01±1.80
GJ 2006B	...	...	...	+4.05±0.23	−1.10±0.06	−32.02±1.82
SCR 0103-5515ABC	...	...	...	+10.93±0.70	−19.50±1.26	−41.64±2.68
LP 467-16AB	−12.34± 1.16	−16.58± 1.19	−9.87± 0.72	−9.55±0.37	+11.37±0.44	−16.01±0.62
GJ 2022A	−7.71± 1.36	−26.52± 1.47	−13.93± 1.02	−0.85±0.03	−4.24±0.14	−24.95±0.81
GJ 2022C	−6.72± 1.36	−25.58± 1.51	−15.12± 2.67	−0.85±0.03	−4.24±0.14	−24.95±0.81
GJ 2022B	−6.55± 1.36	−26.10± 1.45	−13.92± 0.56	−0.86±0.03	−4.24±0.14	−24.95±0.81
LP 993-115	...	...	...	−1.28±0.02	−5.27±0.08	−10.08±0.16
LP 993-116AB	...	...	...	−1.28±0.02	−5.27±0.08	−10.08±0.15
G 7-34	...	...	...	−11.95±0.21	−0.96±0.02	−6.52±0.11
G 39-29A	−40.54± 1.19	−14.62± 0.84	+6.88± 0.82	−12.89±0.33	+1.84±0.05	−2.87±0.07
G 39-29B	−32.71± 1.57	−15.74± 0.86	+8.62± 0.85	−12.89±0.33	+1.84±0.05	−2.87±0.07
LP 655-48	−30.67± 0.33	−14.73± 0.47	−1.84± 0.47	−7.69±0.05	−3.12±0.02	−5.09±0.03
LP 476-207ABC	−10.12± 3.47	−13.55± 1.50	−9.10± 1.77	−23.15±1.19	−4.30±0.22	−8.06±0.42
BD-21°1074BC	−12.92± 1.07	−17.06± 0.99	−11.06± 0.93	−12.01±0.30	−11.00±0.28	−10.25±0.26
BD-21°1074A	−12.37± 0.57	−16.07± 0.54	−8.06± 0.50	−12.01±0.30	−11.00±0.28	−10.24±0.26
L 449-1AB	...	...	...	−5.07±0.08	−8.47±0.14	−6.56±0.11
SCR 0529-3239	...	...	...	−12.41±0.52	−18.83±0.79	−13.28±0.56
SCR 0613-2742AB	−12.43± 0.65	−16.42± 0.90	−9.34± 0.45	−15.99±0.47	−22.49±0.66	−10.07±0.30
L 34-26	...	...	...	+3.16±0.07	−9.22±0.21	−4.16±0.09
SCR 0757-7114	...	...	...	+4.91±0.21	−20.11±0.87	−7.74±0.34
SCR 1012-3124A	−14.59± 1.34	−17.80± 0.63	−7.61± 1.23	−2.38±0.22	−50.55±4.75	+18.65±1.75
SCR 1012-3124B	−14.57± 1.34	−17.55± 0.80	−7.70± 1.24	−2.38±0.22	−50.55±4.75	+18.65±1.75
TWA 8B	−14.10± 0.98	−18.15± 0.74	−6.54± 1.01	+8.21±0.39	−38.65±1.84	+25.44±1.21
TWA 8A	−14.20± 0.39	−17.67± 1.83	−6.85± 1.03	+8.21±0.39	−38.65±1.83	+25.44±1.21
SCR 1214-2345	...	...	...	+3.22±0.06	−7.96±0.14	+6.79±0.12
G 165-8AB	−10.17± 0.87	−22.38± 1.26	−3.81± 6.42	+1.88±0.08	+2.16±0.09	+17.79±0.76
SCR 1425-4113AB	−10.95± 1.24	−16.35± 1.43	−8.85± 0.86	+49.64±3.19	−39.70±2.55	+20.97±1.35
GJ 1224	−28.98± 1.65	−30.09± 0.57	+12.77± 0.45	+7.64±0.06	+1.87±0.02	+0.30±0.01
G 141-29	...	...	...	+7.84±0.16	+7.68±0.16	+1.58±0.03
SCR 1942-2045	+1.08± 0.20	−11.11± 0.25	−2.28± 0.20	+14.14±0.20	+4.94±0.07	−5.50±0.08
2MASS 2009-0113	...	...	...	+7.50±0.13	+6.51±0.11	−3.20±0.05
SCR 2010-2801AB	...	...	...	+40.83±2.63	+10.28±0.66	−22.93±1.48
LEHPM2-0783	...	...	...	+12.46±0.21	−4.76±0.08	−9.11±0.15
L 755-19	...	...	...	+14.02±0.44	+9.24±0.29	−8.46±0.27
SCR 2033-2556	...	...	...	+38.49±2.66	+12.69±0.88	−26.32±1.82
SCR 2036-3607	...	...	...	+12.96±0.29	+1.45±0.03	−9.43±0.21
GJ 799A	−7.99± 2.40	−17.47± 0.65	−9.01± 1.84	+7.80±0.06	+1.54±0.01	−5.85±0.04
GJ 799B	−9.30± 2.40	−13.86± 0.65	−11.49± 1.84	+7.80±0.06	+1.54±0.01	−5.85±0.04
LHS 3799	−0.02± 0.61	−24.92± 0.60	−8.95± 0.94	+3.20±0.04	+2.74±0.04	−5.92±0.08
GJ 1284AB	...	...	...	+3.40±0.10	+3.85±0.11	−14.31±0.40
LHS 1302	...	...	...	−3.98±0.08	+1.48±0.03	−8.97±0.17
LHS 1358	...	...	...	−8.04±0.25	+2.60±0.08	−12.78±0.40
G 99-49	−24.82± 0.64	−16.29± 0.37	+1.05± 0.31	−4.69±0.05	−2.15±0.02	−0.92±0.01
AP Col	−22.00± 0.37	−13.46± 0.36	−4.65± 0.45	−3.72±0.03	−6.70±0.06	−3.41±0.03
G 41-14ABC	+16.03±12.28	−5.62±10.37	+1.62±10.10	−4.38±0.06	−3.70±0.05	+3.60±0.05
TWA 27A	−10.33± 2.88	−15.76± 2.30	−5.14± 2.35	+19.66±0.38	−44.60±0.87	+20.23±0.40
LHS 2729	...	...	...	+7.53±0.16	−8.38±0.18	+8.30±0.18
LHS 2836	...	...	...	+6.65±0.06	−4.83±0.05	+6.96±0.07
GJ 1207	+6.19± 1.44	−0.83± 0.57	−24.39± 0.82	+7.72±0.10	+2.05±0.03	+3.38±0.04
LHS 4016AB	+72.89± 2.85	+4.57± 1.15	−9.44± 0.85	+5.20±0.20	+2.66±0.10	−23.53±0.88

NOTE.—Six-dimensional phase space positions for the stars in this sample.

TABLE 10
MULTIPLE STAR PARAMETERS

Primary Name (1)	Secondary Name (2)	Separation (arcsec) (3)	Position Angle (°) (4)	Ref. (5)	Δmag (6)	Filter (7)	Ref. (8)	Period (9)	Ref. (10)	Resolving Obs. (11)
G 131-26 A	G 131-26 B	0.111	169.9	2	0.46	MKO K_s	2	∼4 y.	2	AO
GJ 2006 A	GJ 2006 B	17.9	4.9	1	0.46	Johnson V	1	...	...	VB
SCR 0103-5515 A	SCR 0103-5515 B	0.249	61.0	3[a]	0.20	2MASS K_s	3	...	...	AO
SCR 0103-5515 AB	SCR 0103-5515 C	1.77	336.1	3	4.43	2MASS K_s	3	...	...	AO
LP 467-16 A	LP 467-16 B	0.409	147.2	2	0.69	MKO K_s	2	...	...	AO
GJ 2022 AC	GJ 2022 B	37.2	78.8	1[a]	1.94	Johnson V	1[a]	...	...	VB
GJ 2022 A	GJ 2022 C	1.8	224.4	1	0.08	Johnson V	1	...	...	VB
LP 993-115	LP 993-116 AB	44.8	60.9	1[a]	0.31	Johnson V	1[a]	...	...	VB
LP 993-116 A	LP 993-116 B	0.257	214.6	4	0.87	SDSS i'	4	...	...	LI,PB
G 39-29 A	G 39-29 B	0.87	300.6	5	0.37	Altair K_s	5	...	...	AO
LP 476-207 AC	LP 476-207 B	1.0	165	6	1.03	CIT K	6	...	...	SP
LP 476-207 A	LP 476-207 C	...	...	...	...	...	...	12 d.	7	SB
BD-21°1074 A	BD-21°1074 BC	8.3	229.3	1[a]	0.67	Johnson V	1[a]	...	...	VB
BD-21°1074 B	BD-21°1074 C	0.760	148.2	1	0.94	FGS F583W	1	...	...	VB,FGS,PB
L 449-1 A	L 449-1 B	0.047	332.8	1	0.95	FGS F583W	1	∼2.5 y.	1	FGS,PB
SCR 0613-2742 A	SCR 0613-2742 B	0.093	...[c]	1	0.59	FGS F583W	1	>4 y.	1	FGS,PB,SB
G 41-14 AB	G 41-14 C	0.62	...	7[a]	0.5	MKO K	7	∼10 y.	7	AO
G 41-14 A	G 41-14 B	...	...	...	...	...	...	7.6 d.	7	SB
SCR 1012-3124 A	SCR 1012-3124 B	1	270	1[b]	0.03	Johnson V	1[b]	...	...	VB,SB
TWA 8A	TWA 8B	13.1	184.7	1	2.97	Johnson V	1	...	...	VB
TWA 27A	TWA 27B	0.778	125.8	8	4.98	2MASS K_s	8	...	...	AO
G 165-8 A	G 165-8 B	0.17	253.3	2	0.16	MKO K_s	2	...	...	AO
SCR 1425-4113 A	SCR 1425-4113 B	...	...	...	...	...	...	...	1	SB
SCR 2010-2801 A	SCR 2010-2801 B	0.614	281.6	1	0.23	FGS F583W	1	...	...	FGS
GJ 803	GJ 799 AB	4681.0	212.4	1[a]	1.71	Johnson V	1[a]	...	...	VB
GJ 799 A	GJ 799 B	2.3	156	1	0.04	Johnson V	1	...	...	VB,PB
GJ 1284 A	GJ 1284 B	...	...	...	...	...	...	...	9	SB
LHS 4016 A	LHS 4016 B	...	...	...	...	...	...	<20 d.	10	SB

NOTE.—VB= Visual Binary. SB = Spectroscopic Binary. PB= Astrometric Binary with perturbation in CTIOPI data. AO= Resolved by AO. LI= Resolved by Lucky Imaging. SP= Resolved by Speckle Interferometry. FGS= Resolved by FGS Interferometry. References: (1) This work; (2) Beuzit et al. (2004); (3) Delorme et al. (2013); (4) Bergfors et al. (2010); (5) Daemgen et al. (2007); (6) Henry et al. (1997); (7) Delfosse et al. (1999); (8) Chauvin et al. (2004); (9) Torres et al. (2006); (10) Shkolnik et al. (2010)

[a]Relative to unresolved components.

[b]Estimate from PSF peaks.

[c]Ambiguous sign on X-axis of solution.

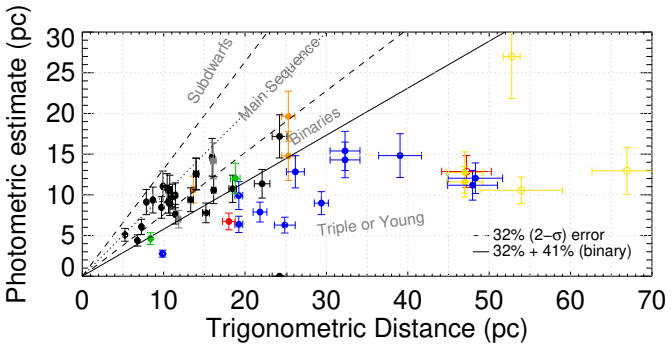

Fig. 1.— A diagram of the 51 resolved components of the 45 systems in this paper, demonstrating their overluminosity in terms of their trigonometric distances (X axis) and photometric distances (Y axis). Objects are color-coded by the association to which they are ultimately linked as members: TW Hydrae are shown in yellow; β Pictoris in blue; Tucana-Horologium, Columba, and Carina in red; Argus in green; AB Doradus in orange; and Castor and Ursa Major in gray. Open circles have no RASS detection.

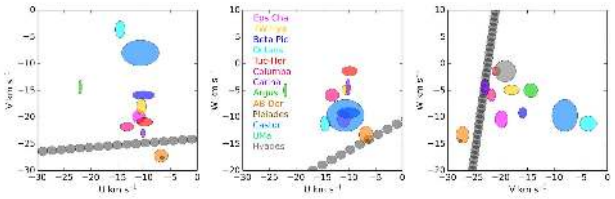

Fig. 2.— Kinematic UVW diagrams for G 7-34. Because we have no radial velocity for G 7-34, UVW velocities (gray) have been calculated for a range of input radial velocities, producing the "string of pearls" effect. The only possible agreement is with the AB Doradus association, with a best-fit radial velocity of +18.0 km s^{-1} (which is suggestive, but not necessarily correct). A similar analyses were carried out for all stars without known radial velocities.

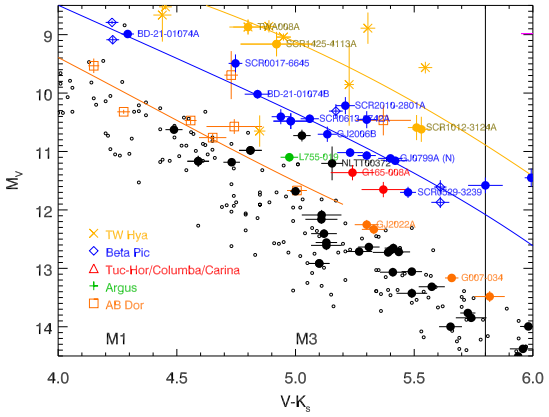

Fig. 3.— The known components of the 45 systems described in this paper (excepting the extremely red objects TWA 27AB, LP 655-48, and SCR 0103-5515C), deblended where necessary and plotted relative to the RECONS 10 pc sample (open circles) on two overlapping color-magnitude diagrams. Also plotted are members of nearby young associations: TW Hya (Xs), β Pic (diamonds), Tuc-Hor (triangles), and AB Dor (squares). Fifth order fits are plotted for (top to bottom) TW Hya, β Pic, and AB Dor. The line at $V - K_S$=5.8 is roughly the point at which M dwarfs are expected to become fully convective.

TABLE 11
DEBLENDING RATIOS

Desired	Observed								
	ΔV_J	ΔR_{KC}	ΔI_{KC}	$\Delta g'_{APASS}$	$\Delta r'_{APASS}$	$\Delta i'_{APASS}$	ΔJ_{2MASS}	ΔH_{2MASS}	ΔK_{S2MASS}
ΔV_J	1.00	1.06	1.36	1.03	1.07	1.28	1.67	1.73	1.80
ΔR_{KC}	0.94	1.00	1.11	1.19	1.03	1.12	1.41	1.46	1.53
ΔI_{KC}	0.74	0.90	1.00	0.97	1.03	1.10	1.26	1.31	1.37
$\Delta g'_{APASS}$	0.97	0.84	1.03	1.00	1.04	1.24	1.38	1.38	1.43
$\Delta r'_{APASS}$	0.93	0.97	0.97	0.96	1.00	1.18	1.32	1.31	1.36
$\Delta i'_{APASS}$	0.78	0.89	0.91	0.81	0.85	1.00	1.11	1.10	1.14
ΔJ_{2MASS}	0.60	0.71	0.79	0.72	0.76	0.90	1.00	1.03	1.07
ΔH_{2MASS}	0.58	0.68	0.76	0.72	0.76	0.91	0.97	1.00	1.04
ΔK_{S2MASS}	0.56	0.65	0.73	0.70	0.74	0.88	0.93	0.96	1.00

NOTE.—Deblending ratios, in the sense of $\Delta Y = n \times \Delta X$ ($\Delta V_J = 1.80 \Delta K_{s2MASS}$). Errors on the ratios themselves are ± 0.03; residuals of the fits are 0.5. V_J data were taken from Bessell (1990, 1991), Weis (1993, 1996); Weis et al. (1999), Koen et al. (2002), and previous papers in this series. $R_{KC} I_{KC}$ were taken from only the Bessell papers. $g'r'i'$ were taken from APASS DR6. JHK_s were taken from the 2MASS Point Source Catalog (Cutri et al. 2003). Parallax data were taken from the RECONS 25 pc Database, which is being prepared for publication.

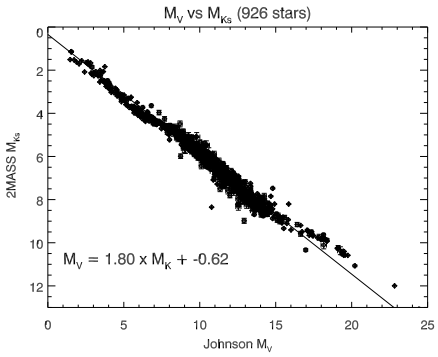

Fig. 4.— The approximately linear relationship between Johnson M_V and 2MASS M_{K_S}, as determined from 962 stars with trigonometric parallax errors less than 10 mas. The values here can be used to convert Δ V measurements into ΔK_s and vice versa. V data from Bessell (1990, 1991), and previous papers in this series; K_S data from 2MASS (Cutri et al. 2003). Other relations are given in Table 11.

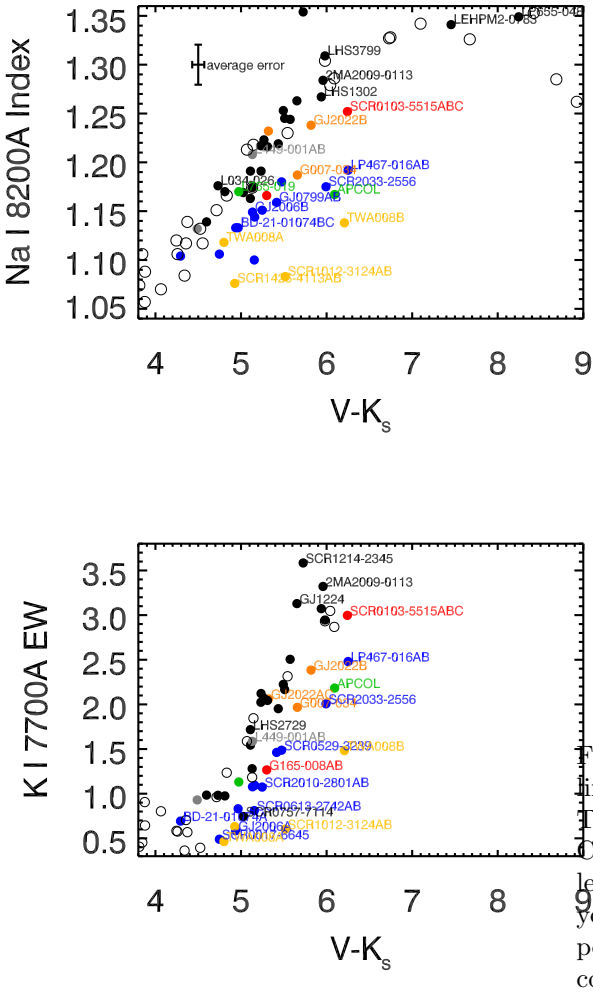

Fig. 5.— The Na I 8183/8195Å doublet gravity index from Lyo et al. (2004b) (above) and K I 7699Å EW (below) vs $V - K_S$ color. Open circles are known main-sequence stars from other RECONS spectroscopic efforts, for comparison. The stars are colored by the association (if any) they appear to belong to: TW Hya (Yellow), β Pic (Blue), Tuc-Hor/Columba/Carina (Red), Argus (Green), AB Dor (Orange), Castor/UMa/Hya (Gray), Field (Black).

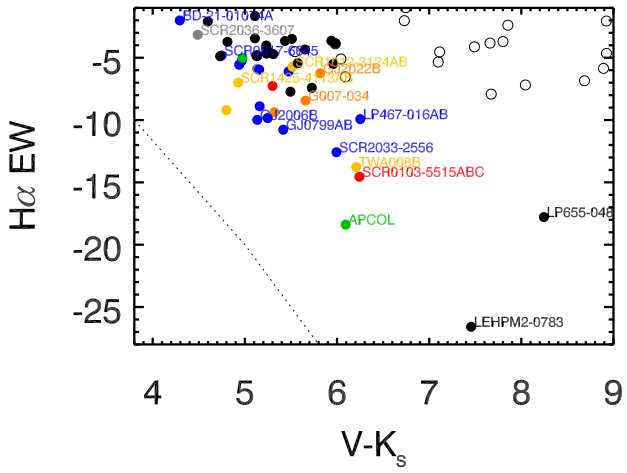

Fig. 6.— Hα EW versus $V-K_S$ color. The dashed line is (roughly) the dividing line between Classical T Tauri stars, as defined in White & Basri (2003). Classical T Tauri stars would appear in the lower left, below the line; none of the stars (even known young stars like RX 1132-2651AB=TWA 8AB) are potential Classical T Tauri stars. The stars are colored by the association (if any) they appear to belong to: TW Hya (Yellow), β Pic (Blue), Tuc-Hor/Columba/Carina (Red), Argus (Green), AB Dor (Orange), Castor/UMa/Hya (Gray), Field (Black). Open circles are main-sequence stars from other RECONS spectroscopic efforts.

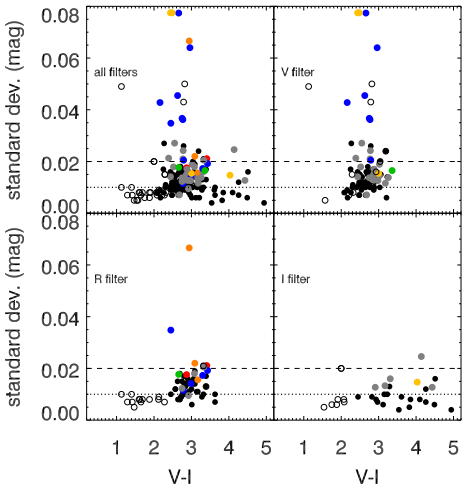

Fig. 7.— A plot of the relative variability of the stars in this paper (closed symbols, colored as in previous figures), compared to previously published CTIOPI stars (black open symbols), as in Jao et al. (2011). Note the different scale from Jao et al. (2011). Our variability "floor" is 0.007 mag, so 0.020 mag clearly indicates a variable star.

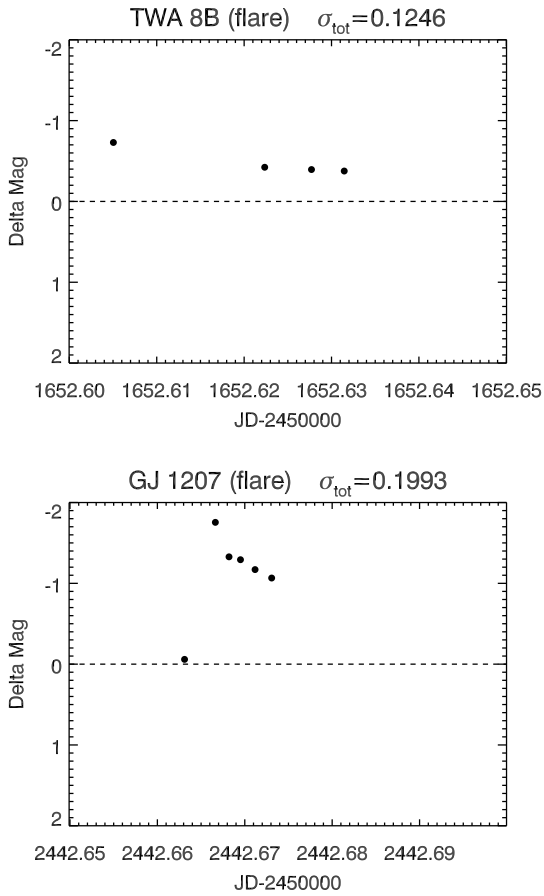

Fig. 8.— Two large partial flares observed in CTIOPI; Note the timescales of the observations and the magnitude spreads; each was observed for less than an hour. We observed the peak of the GJ 1207 flare from 2002 Jun 17 (which rose in less than 5 minutes), but probably not the peak of the TWA 8B flare from 2000 Apr 18. Given that each was observed for less than an hour, it is difficult to tell which had a higher peak, was longer-lasting, or had more total energy. The σ_{tot} scatter values given in Table 2 and Table 6 are highly biased by these flare events. The zero point of the delta magnitudes were set by the other reference stars in the astrometric solution.

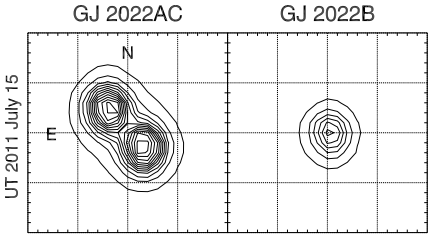

Fig. 9.— Contour plot of GJ 2022A (South) and C (North) on 2011 Jul 15 from CTIOPI. GJ 2022B (37.8″ distant) is also plotted as an example single-star PSF, with the same contour intervals. Grid lines are 2.005″ apart (5 pixels at the CTIO 0.9m).

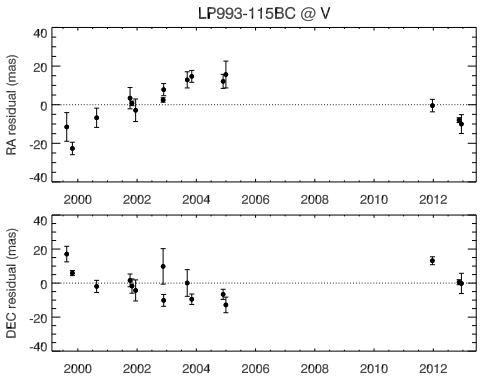

Fig. 10.— Nightly mean residuals of the LP 993-115BC (LP 993-116AB) parallax fit (after the parallax and proper motion have been removed) show a clear astrometric perturbation in both R.A. and Decl. axes. This system is a known binary, but the orbit has not wrapped, and our orbit fit does not converge.

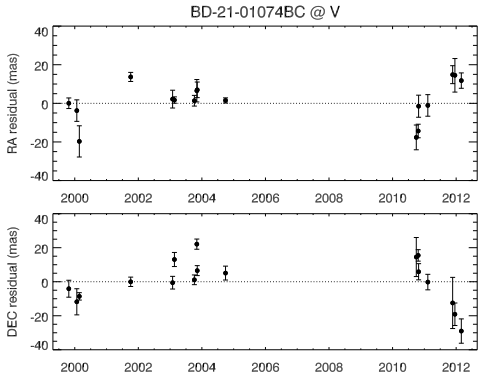

Fig. 11.— Nightly mean residuals of the parallax fit (after the parallax and proper motion have been removed) show a clear astrometric perturbation in both R.A. and Decl. axes. This system is a known binary, but the orbit has not wrapped, and our orbit fit does not converge.

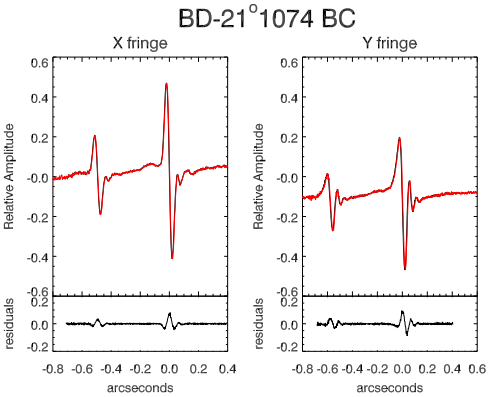

Fig. 12.— The X-axis (left) and Y-axis (right) Hubble Space Telescope Fine Guidance Sensor preliminary results for BD-21°1074BC. Both axes show the pronounced presence of a second component (note that the axes shown here are not R.A. and Decl., but rather the FGS 1r axes at the time of the observation. The quoted position angles elsewhere have been corrected for spacecraft roll angle). Lower panel shows the residuals to the fit; the subtraction is not perfect.

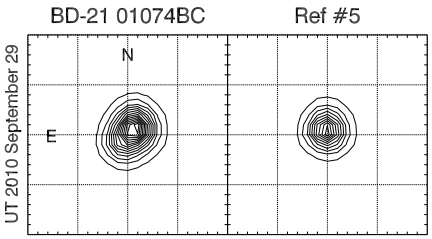

Fig. 13.— Contour plot of BD-21°1074BC on 2010 Sep 29 from CTIOPI data; the SE elongation is probably the C component, despite WDS claiming the position angle is 321°. The nearest reference star (#5) is plotted as a representative single-star PSF, with 4× smaller contour intervals. BD-21°1074A is saturated on this frame and not shown. Grid lines are 2.005″ apart (5 pixels at the CTIO 0.9m).

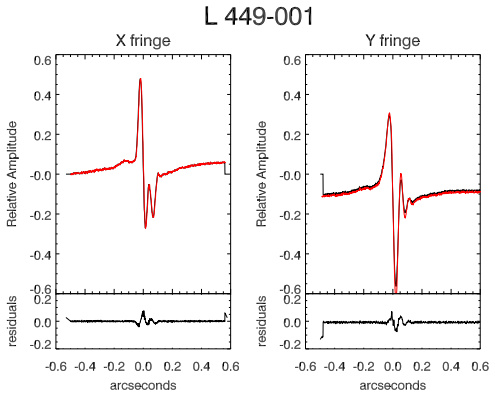

Fig. 14.— The X-axis (left) and Y-axis (right) Hubble Space Telesecope Fine Guidance Sensor preliminary results for L 449-1AB. The X-axis "S-Curve" of the Fine Guidance Sensor shows a second dip to the right of the main one, revealing a companion. The residuals to the fit (bottom) demonstrate that the companion is not readily resolved in the Y-axis S curve.

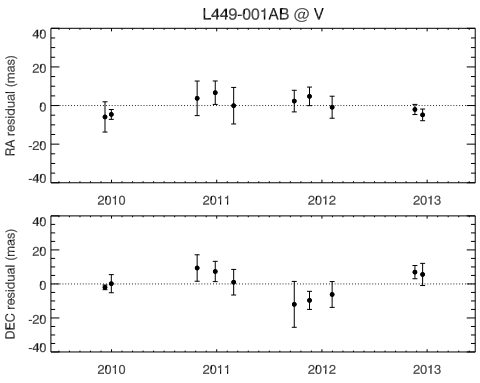

Fig. 15.— Nightly mean residuals of the parallax fit (after the parallax and proper motion have been removed) show an astrometric perturbation in both R.A. and Decl. axes. The CTIOPI data may cover a full orbit, but the astrometric signal is weak.

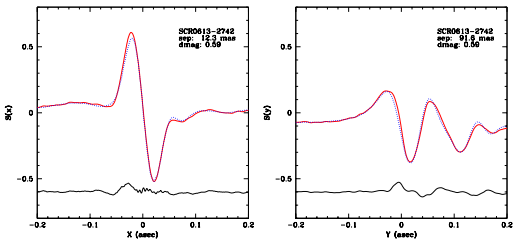

Fig. 16.— The X-axis (left) and Y-axis (right) Hubble Space Telescope Fine Guidance Sensor results for SCR 0613-2742AB. The Y-axis "S-curve" of the Fine Guidance Sensor shows a second dip to the right of the main one (compare to the axes of L 449-1AB, Figure 14), revealing a companion. The companion is also barely resolved at ±12 mas (near the limit of FGS's capabilities) in the X-axis, though this is not visibly apparent, and carries a sign ambiguity.

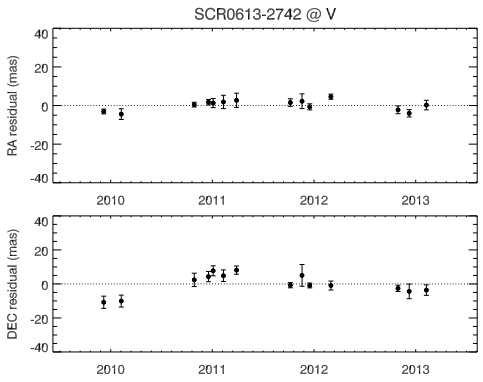

Fig. 17.— Nightly mean residuals of the parallax fit (after the parallax and proper motion have been removed) show an astrometric perturbation in both R.A. and Decl. axes. We have resolved this binary with FGS, but we do not yet have an orbit.

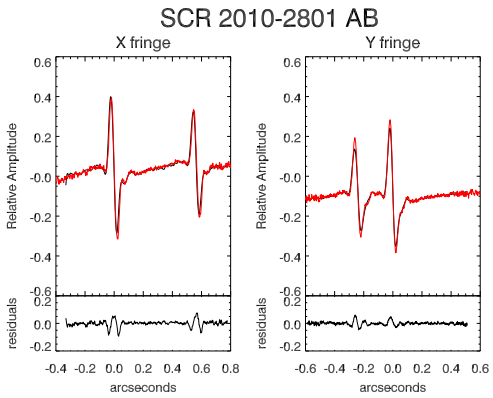

Fig. 19.— The X-axis (left) and Y-axis (right) Hubble Space Telescope Fine Guidance Sensor results for SCR 2010-2801AB. The dual "S-curves" of the two components, originally resolved by Beuzit et al. (2004), are easily visible. The residuals, on the bottom, demonstrate the quality of the fit.

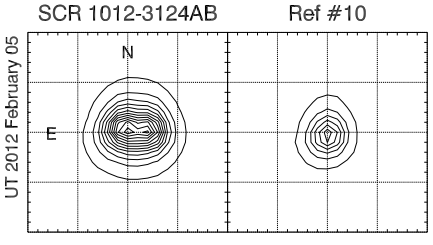

Fig. 18.— Positions of SCR 1012-3124A (E) and B (W) on a rare night when the binary is detectable in CTIOPI data. Reference star #10 is also plotted for a comparison of a single-star PSF from the same night, with the same contour intervals. Grid lines are 2.005″ apart (5 pixels at the CTIO 0.9m).

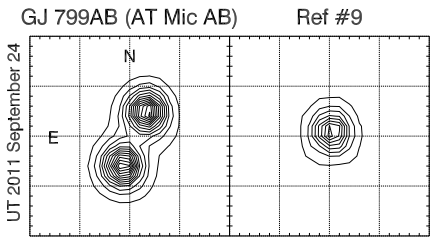

Fig. 20.— GJ 799 A (N) and B (S) on 2011 Sep. 24 from CTIOPI data. The nearest reference star (# 9) is plotted as an example of a single-star PSF, with 800× smaller contour intervals. Grid spacings are 2.05″, 5 pixels at the CTIO 0.9m.